lubricants

MDPI

Review

Solid Lubrication with MoS_2: A Review

Mohammad R. Vazirisereshk [1], Ashlie Martini [1], David A. Strubbe [2] and Mehmet Z. Baykara [1,*]

[1] Department of Mechanical Engineering, University of California Merced, Merced, CA 95343, USA
[2] Department of Physics, University of California Merced, Merced, CA 95343, USA
* Correspondence: mehmet.baykara@ucmerced.edu

Received: 13 June 2019; Accepted: 28 June 2019; Published: 2 July 2019

Abstract: Molybdenum disulfide (MoS_2) is one of the most broadly utilized solid lubricants with a wide range of applications, including but not limited to those in the aerospace/space industry. Here we present a focused review of solid lubrication with MoS_2 by highlighting its structure, synthesis, applications and the fundamental mechanisms underlying its lubricative properties, together with a discussion of their environmental and temperature dependence. The review also includes an extensive overview of the structure and tribological properties of doped MoS_2, followed by a discussion of potential future research directions.

Keywords: MoS_2; solid lubricant; tribology; friction; wear; lubrication; dopant

1. Introduction

With their notable influence on an overwhelming number of natural and technical processes, friction, wear and lubrication are subjects worthy of intense scientific investigation. Despite their importance, studying individual aspects of these phenomena (which are influenced by a multitude of factors including the structural, mechanical, and chemical properties of the involved surfaces) in an isolated fashion has been a challenging endeavor. Nevertheless, with improved computational and experimental techniques, tribology (a term coined in the 1960s that describes the study of friction, wear and lubrication) is now an active field of inquiry, with research groups around the world working on understanding and utilizing its various aspects [1,2].

Considering that a few percent of the gross domestic product of a developed nation is wasted on overcoming the negative impacts of friction and wear (in the form of direct loss of useful energy as well as replacement costs associated with machine components damaged by wear) [3], a major goal of tribology research involves the design and application of methods to minimize friction and wear at interfaces in relative motion. Toward this goal, significant effort is spent on (i) understanding the properties and improving the usefulness of existing lubricants and (ii) coming up with new ways of lubricating interfaces in a more effective fashion (e.g., by decreasing the coefficient of friction, reducing the wear rate and improving the lifetime of components).

Liquid lubricants are typically what comes to mind when one thinks of lubrication in an industrial setting [4]. It is indeed true that oils and greases are conventionally employed in many mechanical systems for lubrication purposes, mostly due to the robust reduction in friction and wear rate that they provide, the ease with which they can be replenished and the straightforward manner with which they can be applied to a variety of surfaces. However, certain operating conditions strictly require the use of solid lubricants instead [5]. The most common examples involve aerospace/space applications, where low temperatures preclude the use of liquid lubricants which simply become too viscous for effective lubrication or may even solidify [6,7]. In fact, most of the technical progress involving solid lubricants was achieved in the second half of the 20th century, motivated by the advent of the space age. Other

examples of applications for solid lubricants involve dry machining operations, where the use of solid lubricants on machine tools (mainly for wear reduction purposes) may significantly cut down on the cost of using large amounts of liquid lubricants, and also the food processing and textile industries, where contamination by liquid lubricants may pose health hazards [8]. In general, solid lubricants are suitable for many applications that operate in conditions too extreme for liquid lubrication.

Among solid lubricants currently in use, molybdenum disulfide (MoS_2) [9] holds special importance. Being a lamellar solid material that consists of individual atomically-thin planes that can easily slide against each other, the use of MoS_2 as a solid lubricant in modern technology dates back to the previous century [10]. Like graphite (another lamellar material), MoS_2 can be used as a dry lubricant by itself, as an additive in oils or greases, or as an individual component of a composite coating [2]. Unlike graphite, MoS_2 does not require humid environments to perform well and it has indeed been shown that its lubricative properties improve drastically in oxygen-deficient environments [11]. Combined with its ability to operate reliably in a wide range of temperatures (from the cryogenic regime to several hundred degrees Celsius), the ability to function effectively in vacuum makes MoS_2 a particularly attractive lubricant for aerospace/space applications. Consequently, a great body of scientific work exists on the synthesis, properties and applications of MoS_2 as a solid lubricant and reviews as well as books on the topic have been published as early as the 1960s (see, e.g., [8,9,12,13]). However, there is still active research on understanding and improving the lubricative properties of MoS_2, with some of the recent focus areas being on its incorporation into (nano-)composite coatings and improving its properties via controlled doping [14,15].

This review provides a focused overview of the tribology of MoS_2 in the form of a snapshot of our current physical understanding of this exciting solid lubricant, with the hope that it could potentially guide future fundamental work. In alignment with this mindset, we focus specifically on MoS_2 by itself as a solid lubricant and do not cover the rather extensive body of work related to its use as an additive in oils and greases or its utilization in (nano-)composite coatings. Specifically, Section 2 describes the structure and synthesis of MoS_2, while Section 3 includes an overview and specific examples of its applications as a solid lubricant. Section 4 details the fundamental mechanisms of low friction and wear associated with the material, followed by Section 5 which discusses the environmental and temperature dependence of its lubricative properties. Section 6 deals with doped MoS_2 and, finally, Section 7 concludes the review by providing a brief summary along with highlights of some of the emerging research directions for MoS_2 as a solid lubricant.

2. Structure and Synthesis

MoS_2 belongs to the family of layered two-dimensional transitional metal dichalcogenides (TMDs). Like graphite and hexagonal boron nitride, its crystal structure consists of covalently bonded sheets, which form stacks that are held together only by weak van der Waals interactions [16]. It occurs naturally as the mineral molybdenite, an important Mo ore. Due to the strong bonding in-plane and weak bonding out-of-plane, mechanical, and other properties are highly anisotropic [17], and the stacks can be easily sheared. Single-layer or few-layer (i.e., 2D) MoS_2 (analogous to graphene) can be produced and studied individually [18].

MoS_2 has several different possible structures (polytypes), depending on the bonding within the sheets and the stacks of the sheets. While graphite has a single plane of atoms per sheet, in MoS_2 each sheet consists of a plane of Mo atoms sandwiched between two planes of S atoms. The single-sheet structure can feature trigonal prismatic coordination around Mo, which is the semiconducting 1H ("hexagonal") structure, or octahedral bonding, which is the metallic 1T ("trigonal") phase. 1H and the ideal 1T each have three atoms (MoS_2) per unit cell (Figure 1); however, theoretical calculations with density-functional theory (DFT) [19] and X-ray diffraction (XRD) experiments [20] have shown that in fact 1T is unstable with respect to distortions. The most commonly reported distorted 1T structure is a reconstruction that triples the unit cell, known as the 1T′ phase [21].

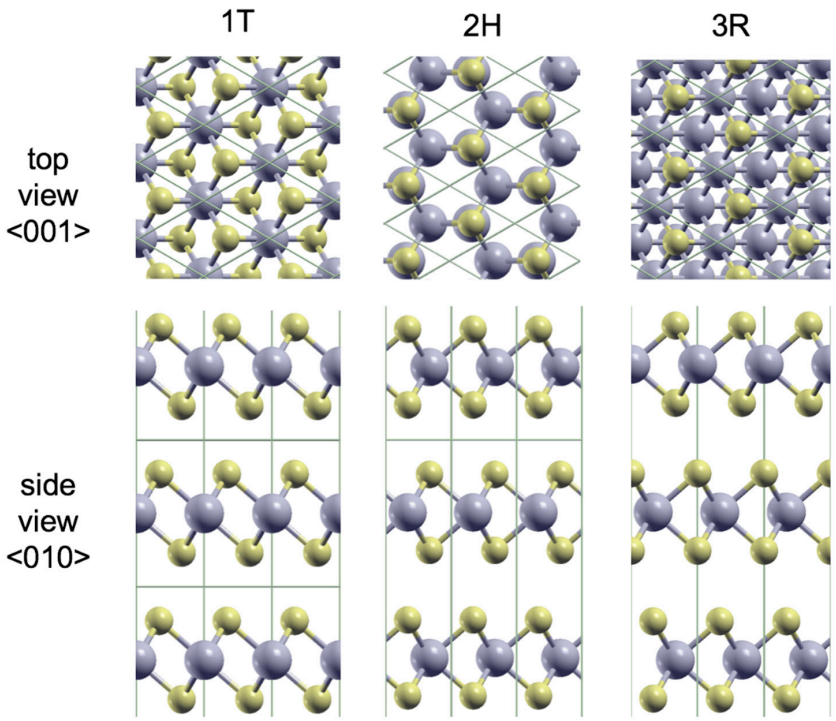

Figure 1. Structures of the polytypes of MoS_2, constructed from the experimental literature, with the conventional unit cell marked for each. For simplicity, the ideal 1T rather than the distorted 1T′ is shown. Mo is gray and S is yellow.

Each single-sheet structure can be stacked into a crystal where the next sheet is exactly above the preceding one (AA stacking), producing the 1H, 1T, and 1T′ polytypes. The naturally occurring polytypes in molybdenite, however, are only based on the 1H sheet, and show more complicated stacking [9]. The more common is the 2H structure with 2 sheets per cell in AB stacking, where an S atom in one layer is above an Mo atom in the layer below [22,23]. The less common 3R ("rhombohedral") structure has three sheets per cell with ABC stacking [22,24]. These structures are shown in Figure 1. Mo-S bond lengths are around 2.4 Å for all polytypes [25]. DFT calculations show only very small energy differences between the 2H and 3R phases [25]. This insensitivity to stacking, and the low surface energy for 2H-MoS_2 of 47 mJ/m^2 = 0.025 eV/cell [26], are indicative of low barriers to sliding and hence low friction. By contrast, 1T and 1T′ are calculated to be higher in energy by 0.8 eV [25] and 0.5 eV per MoS_2 unit, respectively [19].

Lattice parameters and space groups for the polytypes are summarized in Table 1. Nonetheless, deviations from the pristine bulk crystal are common. Calculations have indicated that S vacancies are the most favorable defects in this material [27]. Various kinds of MoS_2 nanostructures can be produced, including nanoclusters [28], nanometer-size sheets [29], nanotubes and even inorganic fullerenes [30]. The nanoparticles often show relatively poor crystallinity in XRD [31]. Amorphous or nanocrystalline MoS_2 has also been reported (see, e.g., [32]).

While the 2H and 3R polytypes of MoS_2 are found in abundance in nature, their bulk single crystals can also be synthesized in the laboratory using the method of chemical vapor transport (CVT), whereby a two-zone quartz furnace is utilized for a duration of multiple days to continuously vaporize parent elemental solids (in this case, Mo and S) in the presence of a catalytic transport agent (mostly halogens), which eventually results in the synthesis of bulk MoS_2 single crystals [33]. Selective synthesis of the 2H and 3R polytypes in CVT can be achieved by the proper choice of transport agent (I_2 for 2H, Cl_2 for 3R) [33]. Despite the fact that the thermodynamically-favored polytypes of MoS_2 (2H and 3R) have been known for a long time, the metastable 1T polytype was only discovered in

the early 1990s, through hydration and subsequent oxidation of alkali-intercalated MoS_2 compounds (most commonly $KMoS_2$) [21].

Table 1. The structures of the three polytypes of MoS_2. In each case, $a = b$, and the unit cell angles are $\alpha = 90°$, $\beta = 90°$, $\gamma = 120°$. Lattice parameters are reported from XRD studies. The 3R structure also has a rhombohedral primitive cell with three atoms.

Polytype	Space Group	Point Group	Atoms Per Conv. Cell	Stacking	XRD Lattice Parameters	Properties
1T′	$P\bar{3}m1$	D_{3d}	9	AAAAAA	a = 5.60 Å, c = 5.99 Å [21]	metallic, metastable
2H	$P6_3/mmc$	D_{6h}	6	ABABAB	a = 3.16 Å, c = 12.29 Å [34]	semiconducting, naturally occurring
3R	R3m	C_{3v}	9	ABCABC	a = 3.17 Å, c = 18.38 Å [34]	semiconducting, naturally occurring

Research on 2D materials has accelerated rapidly in the last decade and a half, thanks to the advent of graphene and the discovery of its exceptional physical properties [35]. Since MoS_2 is one of the layered TMDs, its synthesis/production in 2D form (consisting of single or only a few layers) has also been a subject of intense research. While mechanical exfoliation (i.e., cleaving) through the now-famous adhesive tape method [36] or chemical exfoliation via the use of appropriate solvents [37] and electrochemically-induced bubbling [38] regularly yield 2D MoS_2 flakes of exceptional quality, their lateral size is only limited to a few tens of micrometers and as such, require the establishment of alternative methods for the synthesis of large-scale 2D MoS_2 films for many technological applications. The most promising method toward that direction is chemical vapor deposition (CVD), which entails the use of precursor gases flowing over a substrate (e.g., SiO_2 [39–41], sapphire [42] or Au [43]) at elevated temperatures in a furnace, which eventually results in the synthesis of 2D MoS_2 sheets. With proper choice of precursor gases and deposition parameters, the method now allows the wafer-scale growth and subsequent transfer of high-quality monolayer MoS_2 films for use in various promising applications [44]. Another route toward obtaining 2D films of MoS_2 involves thermal decomposition (i.e., thermolysis) of ammonium thiomolybdate ($(NH_4)_2MoS_4$), which has been demonstrated at the wafer-scale on insulating substrates, with potential use in device applications [45–47].

While 2D MoS_2 films are of potential interest as solid lubricants for nano- and micro-scale mechanical systems, virtually all current applications where MoS_2 is utilized as a solid lubricant involve films/coatings that are significantly thicker (from a few tenths of μm up to a few μm). Traditional methods of applying MoS_2 as a solid lubricant onto solid surfaces include approaches such as burnishing and spray bonding; on the other hand, the great majority of MoS_2 films employed in modern systems are coated onto target surfaces using physical vapor deposition (PVD) and in particular, sputtering. Sputtering involves the bombardment of a MoS_2 target by a noble gas plasma in a vacuum chamber, followed by the ejection and eventual deposition of MoS_2 particles onto the target substrate, creating a conformal coating. The main advantages associated with sputtered MoS_2 films when compared with those obtained by other methods are improved adhesion to the substrate, higher density and significantly higher purity (owing to the deposition process taking place under vacuum), all of which are factors contributing to improved tribological properties including low coefficient of friction and enhanced wear resistance [8]. Sputtered MoS_2 films, which may, in the as-sputtered state, consist of mainly columnar (with MoS_2 crystallites oriented perpendicular to the substrate) or basal (with MoS_2 crystallites oriented parallel to the substrate) morphologies [48], are utilized both for fundamental studies [49] as well as critical applications, e.g., as solid lubricants on bearings employed in spacecraft [7,50]. A particular advantage of the sputtering method is that other materials can be co-sputtered with MoS_2 relatively easily in order to achieve doped coatings with improved properties [15], as discussed further in Section 6. The method of sputtering MoS_2 onto the target surface (in particular, the choice of RF (radio frequency), DC (direct current) and/or

magnetron-assisted sputtering, etc.) can also have important implications for the structure and tribological performance of the resulting films [15]. For example, morphology depends on the deposition system and deposition temperature [51,52]. It has also been shown that sputtering methods as well as substrate bias greatly influence the Mo–to–S ratio in both pure and doped coatings [53,54]. Having said this, a detailed discussion of the relationship between the deposition method and the resulting structure and composition of MoS_2 coatings is not part of this review. Finally, it should be mentioned that alternative methods such as pulsed laser deposition [55] have also been utilized for MoS_2 coatings, although not as widely as sputtering.

3. Tribological Applications of MoS_2

Generally, solid lubricants are used when liquid lubricants do not meet the advanced requirements of a given application. For example, oils or greases cannot be used in many applications because of issues with application, sealing problems, weight, or environmental conditions [56]. Solid lubricants also reduce weight, simplify lubrication and, in some cases, are less expensive than oil and grease lubrication systems [8,56,57]. Table 2 summarizes the conditions and corresponding applications where solid lubricants can be used to overcome limitations associated with standard greases and oils.

In high or ultrahigh vacuum conditions, liquid lubricants can evaporate such that they are unable to perform their lubricating function and can potentially contaminate the device. Similarly, liquid lubricants can decompose or oxidize at high temperatures. At the other end of the spectrum, at cryogenic temperatures, liquid lubricants can solidify or become too viscous to flow effectively. Under radiation or corrosive gas environments liquid lubricants can decompose. High pressure applications can exceed the load carrying capacity of liquids. In cases where contamination is a major issue, liquid lubricants can be problematic because they tend to pick up dust and other contaminants from the environment. In applications where weight is of primary importance, liquid lubricants and the associated components can be too heavy. Lastly, if service is difficult or impossible, it may not be viable to use a liquid lubricant that degrades over time, particularly if the application experiences long storage or idle periods. Solid lubricants overcome many of these issues.

Notable in Table 2 is one application where almost all the conditions for poor liquid lubrication exist, i.e., in space mechanisms. Moving systems in space include vehicles, satellites, telescopes, antennas, and rovers. Such systems must operate for long periods of time with little or no service under a wide range of extreme environmental conditions. Since most space applications operate in vacuum environments, the typical solid lubricant of choice is MoS_2 [7,58]. Unlike graphite, which requires sufficient vapor pressure of water to provide lubrication, MoS_2 performs best in vacuum environments [59]. Representative examples of components in space applications that already rely on MoS_2 lubricants are ball bearings, pointing mechanisms, slip rings, gears, and release mechanisms [15,60]. It has indeed been suggested that most, if not all, the American satellites and spacecraft contain MoS_2 for some application [13].

The continuing interest in the development of solid lubricants (including MoS_2) for space applications stems from the fact that planned space missions increasingly involve a wide range of operating conditions (in particular, in terms of temperature) and longer durations during which the mechanisms that enable relative motion will need to operate in a robust and reliable fashion without regular maintenance. A particularly important example highlighting the importance of related efforts is the catastrophic high-gain antenna deployment failure associated with the Galileo spacecraft [61], caused by the failure of the MoS_2-based solid lubricant during operation in space that was successfully tested before deployment on Earth under ambient conditions. In order to meet the requirements of demanding space missions, basic and applied research is being conducted around the world to understand and improve the properties of solid lubricants in general and MoS_2-based lubricants in particular. Illustrative examples of such ambitious missions include NASA's planned lander mission to Europa (the surface of which can be below −200 °C) for astrobiology research, as well as ESA's BepiColombo mission to Mercury, where the spacecraft will be exposed to temperatures on the order of 250 °C [7].

Table 2. Examples of conditions or environments where liquid lubricants are either undesirable or ineffective and solid lubricants can be used, and representative applications where those conditions exist; adapted from Ref. [56].

	Space Mechanisms	Medical or Dental Equipment	Nuclear Reactors	Food Processing Equipment	Hard Disks, Microscopes, Cameras	Semiconductor Manufacturing	Furnaces/ Metalworking Equipment	Refrigeration/Liquid Nitrogen Pumps	Bridge, Plant or Building Supports
High Temperature	x						x		
Cryogenic Temperature	x							x	
Radiation	x		x						
Corrosive Gas	x					x			
High Pressure/Load	x						x		x
Product Contamination Unacceptable		x		x	x	x			
Service Difficult or Impossible	x		x						
Weight Limited Applications	x								

Based on the fact that MoS_2 is the most extensively used solid lubricant in space mechanisms, a particularly timely example will be highlighted here: the James Webb Space Telescope (JWST), which is planned for launch in 2021 and is the successor to the Hubble Space Telescope. MoS_2 has been determined as the solid lubricant of choice for sensitive mechanisms employed in a number of precision instruments on JWST, including the Near Infrared Spectrograph (NIRSpec) and the Mid-Infrared Instrument (MIRI) (Figure 2) [50,62]. Critical to the choice of MoS_2 as the preferred solid lubricant for these high-precision instruments was the fact that it preserves its lubricative properties down to cryogenic temperatures (which include 30 K, the temperature around which JWST will be operating) [63] and the high uniformity with which it can be deposited on precision bearings employed in the instruments at sub-micron thicknesses, ensuring stable operation. In order to minimize the chances of a lubricant-related catastrophic failure after deployment (like the Galileo), a significant amount of work has been performed to characterize the tribological performance of bearings under various operating conditions on earth and it has been determined that a run-in procedure performed under vacuum is necessary to ensure low-friction torques for eventual use in space [64].

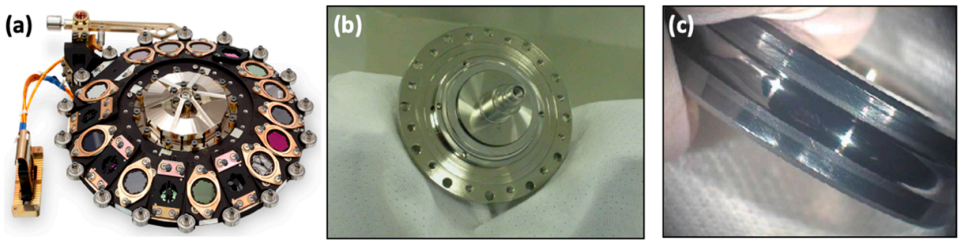

Figure 2. (**a**) The filter wheel assembly of the MIRI instrument on the JWST; (**b**) A bearing employed in the filter wheel assembly; (**c**) The MoS_2-coated bearing race featured in the bearing. (**a**) and (**b**) reproduced from [50] with SPIE permission. (**c**) Republished with permission of IOP Publishing from [7]; permission conveyed through Copyright Clearance Center, Inc.

The impressive tribological properties of MoS_2 under vacuum and in a wide range of temperatures make it a natural choice as a solid lubricant for applications in space; however, the fact that its lubricity rapidly deteriorates under humid conditions represents a significant barrier to its extensive use in demanding terrestrial applications. On the other hand, recent developments in coating technology, in particular the use of closed field unbalanced magnetron sputter ion plating (CFUBMSIP) employed to co-sputter MoS_2 with Ti, has resulted in lubricant coatings with notable improvement in mechanical properties and resistance to humidity [65–67]. These improvements resulted in the successful use of MoS_2-based coatings in dry machining operations, such as cutting and forming, as well as certain machine components that do not operate under vacuum conditions. Despite these developments, it is projected that the main use of MoS_2 as solid lubricant will be in aerospace/space applications for the foreseeable future, with ongoing fundamental and applied research directed at adjusting the properties of MoS_2 coatings toward long-term missions and a wider range of operating conditions.

Before concluding this section, it needs to be mentioned that MoS_2 has numerous other applications besides lubrication that are not covered in this review. One of the most important is heterogeneous catalysis, in which active sites are edges, defects, or near "promoter" dopants (Ni, Co). MoS_2 can catalyze reactions including hydrodesulfurization, hydrogen evolution reaction, oxygen reduction reaction, and photo-catalytic water splitting [68]. The ability of MoS_2 to absorb Li between its layers (intercalation) has been utilized for batteries [68]. Electronic and optical applications have become a particular focus after the advent of few-layer MoS_2, which have been reviewed recently [18,69]. Some unique features are strong excitonic effects, a direct-to-indirect band-gap transition with number of layers, tunability by strain, and ease of creating heterojunctions by stacking. The presence of multiple inequivalent low-energy valleys in the band structure might be used in "valleytronics", and the strong spin-orbit coupling suggests spintronic applications. These properties have been explored for use in transistors, sensors, photovoltaics, light-emitting diodes, and lasers [18,69].

4. Mechanisms of Low Friction and Wear

While MoS_2 has been known to be a good solid lubricant for many years [12], the mechanisms through which this performance is achieved have been a subject of ongoing research. This section will provide an overview of experimental and computational efforts aimed at understanding the physical reasons behind the extraordinary lubricity of this lamellar material. Moreover, key results of atomic force microscopy (AFM) based friction studies on 2D MoS_2 samples (which only consist of a single layer or a few layers stacked on top of each other) will be reviewed.

The most widely-referenced works in the literature aimed at elucidating the lubricative properties of MoS_2 are the detailed transmission electron microscopy (TEM) studies by Martin et al. that were performed in the early 1990s [49,70]. While techniques such as XRD have been employed before to understand some aspects of the friction mechanisms related to MoS_2 coatings [71], the TEM images provided convincing visual evidence for the processes by which MoS_2 was thought to exhibit low friction and wear [49,70]. In particular, by performing pin-on-flat tribometer experiments under ultrahigh vacuum conditions on sputter-deposited, stoichiometric, polycrystalline MoS_2 films followed by TEM imaging of the wear debris as well as the film itself, the following key processes were determined to take place during relative sliding motion between components lubricated by MoS_2:

(1) The establishment of a transfer film on the counter-surface as it slides against the MoS_2-coated component.
(2) The shear-induced orientation of the basal planes of MoS_2 (in the original coating, the transfer film and eventually in third bodies/wear particles) in the sliding direction.

Careful study of the Moiré patterns that emerge during TEM imaging showed that a key feature leading to ultra-low friction (often referred to as superlubricity [72], with friction coefficients on the order of 0.001) of MoS_2 coatings is significant variability in the rotational registry of individual MoS_2 crystallites around the surface-normal direction (Figure 3). This leads to a rotational structural mismatch between basal plane pairs that come into contact with each other at the interfaces that form between the original coating, the transfer film and the third bodies, leading to a systematic cancellation of atomic-scale lateral forces. This results in the establishment of an ultra-low friction regime, in agreement with the theory of structural superlubricity that was spearheaded by Hirano [73] and Sokoloff [74], and is still being investigated in many different experimental systems [72].

Even though the pioneering TEM works described above pinpoint structural superlubricity between basal planes of MoS_2 as the main reason for its ultra-low friction characteristics, a particular limitation involves the inability to directly observe, in an in situ fashion, the sliding process between the layers and to directly measure the shear forces that take place during sliding. These shortcomings were partially addressed in a careful experimental study performed by Oviedo et al., where two custom cross-sectional TEM setups were used to (i) visualize in situ with high-resolution the sliding between individual basal planes of MoS_2 (Figure 4) and (ii) quantify the shear strength of the interface between the layers [75]. In particular, the upper bound for the shear strength was determined (by focusing on interlayer sliding between MoS_2 layers in commensurate registry) to be 24.8 ± 0.5 MPa. In another important work, utilizing a mechanical force sensor in the form of a silicon nanowire inside a scanning electron microscope (SEM), an individual, single-layer flake of MoS_2 was controllably detached from and slid on its bulk parent MoS_2 substrate in structurally incommensurate registry [76]. In what constituted the first direct measurement of friction forces between incommensurate basal planes of MoS_2, the authors obtained an ultra-low friction coefficient on the order of 0.0001 (well within the superlubric regime [77]), supporting the original proposition by Martin et al. that easy-shear sliding between incommensurate basal planes of MoS_2 is responsible for its ultra-low friction. In yet another rather challenging experimental study, AFM tip apexes were intentionally wrapped with sheets of 2D materials (including MoS_2) and slid on a bulk graphite substrate, with experimentally-recorded friction coefficients smaller than 0.002 [78].

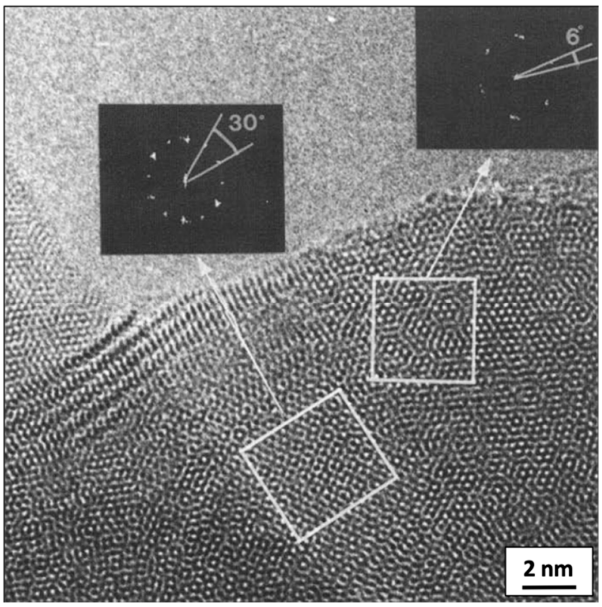

Figure 3. A high-resolution TEM image obtained on MoS_2 wear debris that shows the existence of two separate MoS_2 planes with different rotational registry on the underlying MoS_2 region. Figure reprinted from [70] with permission from Elsevier.

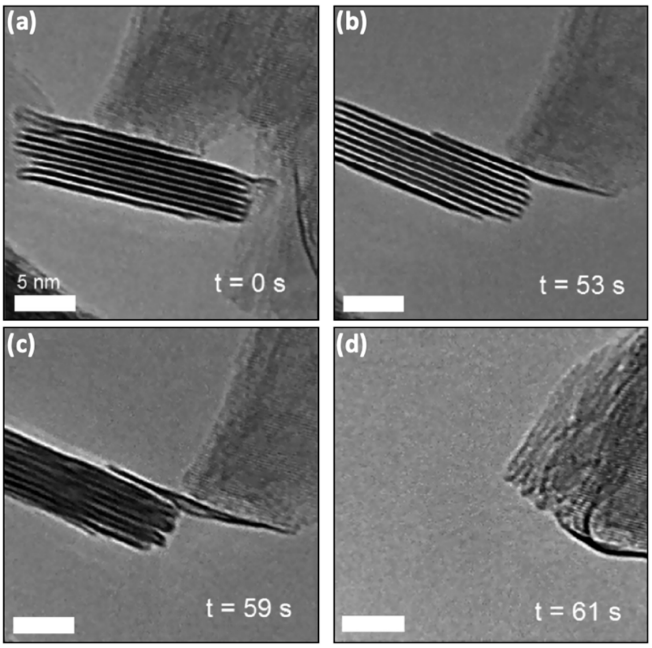

Figure 4. High-resolution, cross-sectional TEM images obtained sequentially over the course of a minute as an oxidized tungsten tip is used to controllably shear off a single layer of MoS_2 from a nine-layer sample. Adapted with permission from [75], copyright 2015 American Chemical Society.

Due to experimental difficulties associated with the measurement of friction forces between individual MoS_2 planes in an isolated fashion and the requirement of highly customized setups that are not readily accessible, computational efforts play an important role in the elucidation of low friction mechanisms of MoS_2. Importantly, simulations of sliding between individual MoS_2 sheets based on molecular dynamics (MD) have uncovered (i) a 100-fold decrease in friction force when the sheets are rotated with respect to each other to transition from a commensurate to an incommensurate state; (ii) that the highest energy barriers to sliding are located on top of S atoms; and (iii) that Coulombic repulsion between the layers plays an important role in the easy shear characteristics, supplementing

the reduction in energy barriers to sliding that is induced by structural mismatch [79,80]. A subsequent study based on DFT focused on the load-dependence of friction between individual MoS_2 planes by simulating potential energy landscapes, and determined that inter-layer friction increases with increasing load based on electrostatic effects [81]. Another study of inter-layer motion using both DFT and MD showed that the energy barriers to sliding in MoS_2 are larger than those of other 2D materials (graphene and boron-nitride) due to the corrugated nature of the MoS_2 surface, which increases both the dispersion binding and the energy barriers, and also because the sulfur anions are more polarizable than the first-row atoms in graphene and boron-nitride [82].

The main characteristics that make MoS_2 a low-friction material (in particular, the ability of its basal planes to orient in the direction of sliding) are also mainly responsible for its wear-resistant properties. TEM-based studies performed on MoS_2 films deposited by CVD have established that mechanical properties including strength, elastic modulus and strain to fracture improve during the initial stages of sliding, accompanied by a marked decrease in wear rate [83]. The physical mechanism behind the in situ enhancement of mechanical properties and thus, wear resistance, is thought to involve an interplay of film densification (induced by individual crystallites pushing into the pores in the as-synthesized films under contact stresses) and the ability of the MoS_2 crystallites to easily re-orient themselves in the direction of sliding to accommodate shear strain and delay the onset of fracture that would eventually manifest as wear [83,84]. The wear resistance of pure MoS_2 films can be further augmented by the use of dopants [85], as described in Section 6.

It is also important to note that the tribological behavior of MoS_2 depends on the test conditions, as reflected in the stability and thickness of the generated tribofilm. The properties of the tribofilm are determined by the conditions at the interface and so are intrinsic to the tribological system. Therefore, one approach to understanding the tribological mechanisms of MoS_2 is to analyze the transfer film. This has been done, for example, using techniques that involve stylus-based roughness measurements on the counterface [86] or using approaches based on digital microscopy to characterize tribofilm evolution [87,88].

The invention of the AFM [89] and the realization that it can be used to study frictional properties on the nanometer scale [90], opened up a new era in tribology research where friction could, for the first time, be studied at the "single asperity" level, with the potential to provide fundamental physical information about this ubiquitous phenomenon. Moreover, the realization that graphene can be readily obtained from its lamellar bulk form by simple mechanical exfoliation [91] and the booming interest in related 2D materials that followed, resulted in a number of AFM-based studies regarding the frictional properties of such materials. The motivation to study the frictional properties of 2D materials is mainly based on the desire to establish robust and effective lubrication schemes for nano- and micro-scale mechanical systems, where increasing surface-to-volume ratios amplify surface effects (e.g., surface tension, stiction) that preclude the use of liquid lubricants and lubrication via thick layers of lamellar solids is generally impractical because of geometric constraints associated with the size of the components.

At this point, it should be emphasized that AFM-based friction studies on 2D materials (including MoS_2) probe mechanisms and properties that are fundamentally different from those that are largely responsible for the lubricity of such materials in their bulk form. In particular, while the excellent frictional properties of MoS_2 have been mainly attributed to easy shear between its basal planes and related processes as discussed above, no interlayer shear takes place during AFM experiments, where the measured friction forces occur at the interface between the AFM tip and the top surface of the MoS_2 sample. Based on this, it is perhaps surprising that AFM-based studies of friction on such materials still reveal miniscule friction forces and drastically decreased friction when compared with typical substrates (e.g., SiO_2) on which they are deposited. As no interlayer sliding takes place during experiments that feature a few-layers of material (and interlayer sliding is, by definition, not possible for single-layer samples), the significant lubricative properties of 2D materials in AFM experiments are

attributed to other physical factors [92], including their (i) atomic-scale smoothness; (ii) mechanical strength and (iii) chemical inertness.

Despite the fact that the great majority of AFM-based nanotribological studies on 2D materials have been performed on graphene, single- or few-layer MoS_2 have also been the target of some recent experimental work. Although AFM-based friction measurements on single-layer MoS_2 have been performed as early as 1996 [93], the first systematic, comparative report of AFM-based friction measurements on 2D materials (which also includes results obtained on mechanically exfoliated flakes of single- and few-layers of MoS_2) appeared in 2010 [94]. Specifically, it was observed that the magnitude of friction measured on MoS_2 (deposited on SiO_2 substrates) decreased monotonically with increasing number of layers (until a total of ~5 layers was reached, see Figure 5). The authors attributed the consistent behavior of decreasing friction with increasing number of layers to a mechanical process called puckering, whereby the AFM tip apex that probes the 2D samples creates locally deformed areas (puckers) around itself, which increases friction due to an increase in contact area. As the number of layers increases, the bending stiffness of the 2D material in the vertical direction also increases, leading to a decrease in puckering and consequently, in friction. While factors, such as electron-phonon coupling [95] as well as surface roughness [96], may also play a role in the layer-dependent friction of 2D materials, the puckering phenomenon is generally accepted to be the dominant mechanism.

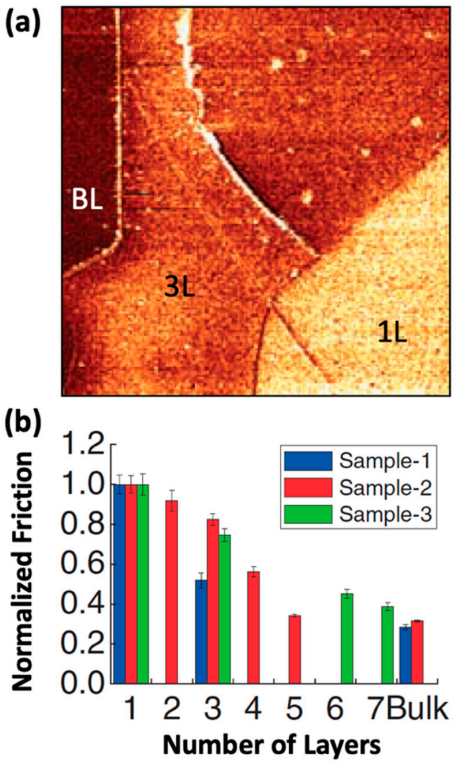

Figure 5. (**a**) Friction map acquired by AFM on an MoS_2 flake featuring regions of single-layer (1L), three-layer (3L) and bulk (BL) thickness. Brighter colors indicate higher friction values; (**b**) Normalized friction as a function of number of MoS_2 layers for three different samples, whereby a decrease in friction with increasing number of layers is observed. The friction map in (**a**) corresponds to Sample 1 in (**b**). Reprinted from [94] with permission from AAAS.

Recent work performed on polycrystalline, single- to few-layer MoS_2 samples grown by CVD featuring grains up to a few hundreds of nanometers in size revealed a strikingly different layer-dependence of friction than single crystal samples obtained by mechanical exfoliation [97]. In particular, under ambient conditions, the layer dependence was found to be of an "oscillatory" nature, whereby samples with odd numbers of layers exhibited higher friction relative to those samples with

even numbers of layers. This rather interesting result was attributed to a mechanism involving the enhanced adsorption of charged species at samples with odd numbers of layers due to the existence of permanent dipoles. The adsorption of such species changes the interactions of the sample surface with the probing tip apex, ultimately leading to enhanced friction when compared with samples featuring even numbers of layers [97].

In AFM experiments, it is widely observed that the physical properties of the tip apex have a profound effect on the recorded data. This observation is also true for AFM-based investigation of friction mechanisms on MoS_2, as it has been recently shown that layer-dependent friction on 2D MoS_2 becomes strongly non-monotonic (first decreasing when switching from one to two layers, and then progressively increasing with increasing number of layers) when probed with blunt, pre-worn tips [98]. These results point to the conclusion that the physical properties of individual sliding components, in addition to those of the solid lubricant, need to be carefully evaluated in the design of small-scale mechanical systems to achieve adequate lubricative performance.

The anisotropy of friction on MoS_2 is another topic that has been investigated via AFM on 2D samples. Specifically, Cao et al. determined, by means of consecutive friction measurements performed on MoS_2 flakes gradually rotated with respect to the AFM scanning direction, that the friction forces on MoS_2 exhibit anisotropic behavior with a periodicity of 180° [99]. This observation is surprising at first glance, as a periodicity of 60° would have been expected based on crystal symmetry. Inspired by previous anisotropy work on graphene [100], the authors attributed their observations to the existence of parallel ripples in the MoS_2 samples induced by in-plane strain that occurs during the deposition of the samples on the SiO_2 substrate in conjunction with the puckering effect, which leads to the emergence of high- and low-friction sliding directions (separated by 90°) that correspond to the tip moving across or along the ripples, respectively. While the work by Cao et al. also discusses the effect of sample thickness and load on friction anisotropy in a convincing fashion, the specific role played by the AFM tip apex (for instance, by its size and stiffness) in friction anisotropy remains to be studied in future work.

The frictional properties of 2D MoS_2 have been recently compared with those of graphene [101], employing samples grown by CVD, which provides films of lateral sizes that are much more suitable for practical purposes than those obtained by mechanical exfoliation. By combining AFM-based imaging and micro-tribometer tests, it was determined that the MoS_2 film exhibited superior friction and wear characteristics when compared with graphene. The authors attributed this observation to the fact that MoS_2 is directly grown on the SiO_2 substrate employed in the measurements, whereas graphene needs to be grown on copper foils first and then transferred onto SiO_2 through chemical means. This process inevitably introduces contaminants, which prevent intimate contact and adhesion between graphene and the underlying substrate, ultimately leading to inferior friction and wear performance [101]. This result is in contrast to another recent direct comparison between MoS_2 and graphene conducted via AFM measurements of both materials in the same scan line that showed graphene consistently exhibited lower friction. The experimental results were analyzed using DFT and MD simulations, which revealed the mechanism underlying the friction contrast to be a higher energy barrier to sliding on MoS_2 [102]. These studies will almost certainly encourage future comparisons between 2D materials which will highlight their strengths and weaknesses and inform their use in specific applications.

5. Environment and Temperature Dependence

The tribological behavior of MoS_2 is extremely sensitive to environmental conditions. As stated before, one of the main prerequisites to achieve ultralow friction with MoS_2 lubricants is the absence of contaminants, such as oxygen, water, and hydrocarbons [49]. Among the first observations of the environmental dependence of the lubricative properties of MoS_2, Peterson and Johnson [103] showed in 1953 that the friction between metal surfaces lubricated by MoS_2 increased with relative humidity (R.H.) up to 65% and then decreased. After this work, the presence of water and various

forms of oxygen was shown to increase friction and wear in several studies [104–108]. In the following, we summarize the effect of oxygen and then water on the friction and wear behavior of MoS_2 as a solid lubricant.

The presence of molecular and atomic oxygen can lead to surface-limited oxidation (or near-surface-limited, due to the subsequent protection that occurs via the oxidation layer) of MoS_2 films, significantly affecting their tribological performance. The oxidized layers of MoS_2 films can cause high friction during the run-in process; then, once the initial oxide has been removed, the friction drops to its low steady-state value as long as the oxide removal rate is higher than the oxidation rate in the system [109,110]. This high friction run-in regime can cause problems particularly in aerospace and satellite devices in which operation is infrequent and oxidation can occur by molecular oxygen during the assembly and testing of a device on earth [111]. Oxidation may also happen in the presence of atomic oxygen, which is extremely reactive and quickly oxidizes the surface of MoS_2 [112], particularly during operation in the low earth orbit (LEO) environment (altitudes of 100–1000 km). The pre-operation exposure to the terrestrial environment before space missions enhances the premature failure risk in satellite devices. The failure of the high gain antenna in the Galileo spacecraft is an example caused by this problem, whereby the failure of bearings during deployment was attributed to the prolonged storage and transportation of the components [113].

Molecular oxygen was shown not to affect the tribological properties of MoS_2 at room temperature [109,114]; however, it can oxidize the MoS_2 edge sites at high temperature, whereby MoO_3 (and MoO_2), as a product of this oxidation, disrupts the easy shear properties of the MoS_2 lubricant film and creates high wear [115]. The oxidation of MoS_2 starts with the physisorption of oxygen on the surface of MoS_2 and then the chemical formation of Mo oxides. MoS_2 oxidation increases with an increase in temperature [116]. The transition temperature at which the oxidation rate increases substantially has been reported to be from 100 [117,118] to 400 °C [119,120], which may depend strongly on the preparation method of the MoS_2 film and on film conditioning induced by deliberate thermal cycling during sliding prior to testing [109]. In general, powdered coatings (i.e., mechanically deposited coatings) exhibit higher transition temperatures compared to sputtered coatings, which might stem from (i) larger grain sizes in the mechanically deposited films which decrease the susceptibility to oxidation and/or (ii) the porous structure of the sputtered films which can speed up the oxidation of MoS_2 as a result of tribochemical reactions [109,119,121,122]. The effect of microstructure on tribological performance of MoS_2 coatings under ambient environment was further studied by comparing the friction of highly oriented N_2-spray-deposited MoS_2 films and amorphous films produced via DC magnetron sputtering [123,124]. Highly-ordered MoS_2 films with surface-parallel basal orientation exhibited higher resistance to oxidation compared to amorphous MoS_2 films. Moreover, X-ray photoelectron spectroscopy (XPS), and high-sensitivity low-energy ion scattering (HS-LEIS) analysis revealed that highly oriented MoS_2 lamellae restricted the oxidation to the first few top layers, which led to a shorter run-in period compared to amorphous MoS_2, where the deeper penetration of oxygen into the surface resulted in a longer run-in period (Figure 6b,d) [124]. Therefore, deposition techniques that result in a lower density of edge sites or highly oriented lamellae of MoS_2 can reduce the possibility of oxidation, thereby minimizing the degradation of tribological performance under ambient conditions.

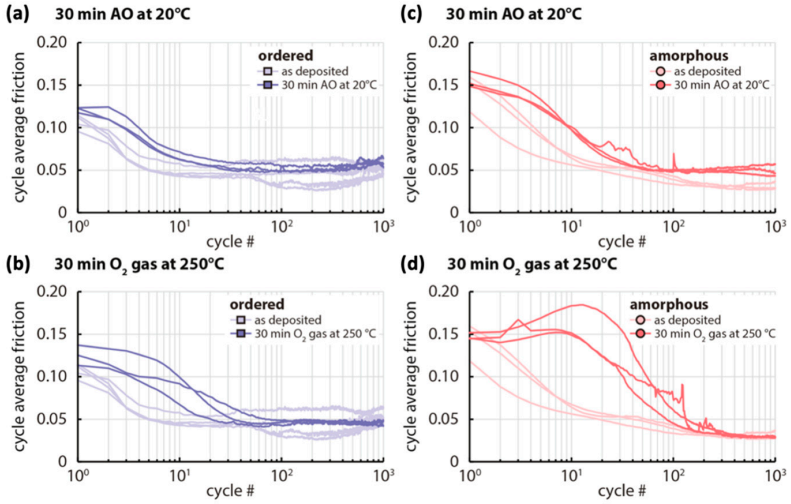

Figure 6. The effect of microstructure on the tribological performance of MoS_2 coatings as illustrated by the friction coefficient as a function of number of cycles for ordered (**a**,**b**) and amorphous (**c**,**d**) MoS_2 films with different exposure times to atomic oxygen (AO) and O_2 at different temperatures. The lighter color in each plot represents the as-deposited coating performance. Adapted with permission from [124], copyright 2017 American Chemical Society.

Atomic oxygen (AO) is an abundant species (with a high flux density on the order of 10^{13}–10^{15} atoms·cm^{-2}·s^{-1} and kinetic energy ~5 eV) that acts on exposed surfaces of devices and components employed in space applications, and can cause deterioration of material properties [125]. There has been extensive research on the effect of AO on the tribological performance of MoS_2 lubricants (see, e.g., [122,125–129]). However, there are some discrepancies in the reported results: for instance, no change in the tribological properties of MoS_2 after AO exposure was reported by [128]; whereas most other studies reported high initial friction due to the limited depth of oxidation, and S loss on the MoS_2 coating surface [125–127,129]. Moreover, Wang et al. observed an overall higher mean friction for a pure MoS_2 sample with AO exposure as well as a direct correlation between the wear-volume/friction and the AO exposure time [122]. The atomic oxygen flux density during sliding has also been shown to inversely affect the life of the coating [127]. The discrepancies in these results might stem from differences in experimental conditions such as atomic oxygen beam energy (thermal to keV), fluence (i.e., intensity, 10^{12}–10^{24} atoms/cm^2), sample preparation and/or tribological test conditions [130].

The effect of a humid environment, i.e., water vapor, on the friction and wear properties of MoS_2 lubricant coatings has been extensively studied since the mid-20th century [12,103,106,107,109,131]. Generally, the presence of water molecules in the environment (e.g., while storing MoS_2 under humid conditions) leads to an increase in sliding friction and wear rate regardless of the MoS_2 film deposition technique employed [13,93,105,132,133]. Despite general agreement in the literature about the effect of water on the tribological behavior of MoS_2, there are discrepancies regarding the governing mechanism associated with this phenomenon. Common hypotheses for the increase in friction in humid environments include:

- Water-driven oxidation of MoS_2 edge sites [104–107,132];
- Physisorption of water molecules at the surface which deteriorates the tribological behavior of MoS_2 via disruption of the easy shear of lamellae [131,133–137], adhesion enhancement [138,139], hydrogen bonding between basal planes of MoS_2 [140,141] and restriction of the growth and reorientation of the tribofilm [123].

For many years, oxidation of MoS_2 at edge sites was thought to be the mechanism responsible for increasing friction and wear rate of MoS_2 under humid environments [104–107,132]. This hypothesis was mainly tested in the presence of both water and oxygen species and an enhancement in oxide

formation (and subsequent sulfur loss at the surface) was observed as the relative humidity (i.e., partial pressure of water) increased. As mentioned before, oxygen alone can oxidize the MoS_2 film, so the important question about the effective and distinctive role of water in oxide formation remained unanswered in these studies. Recent experiments [109,117,131,133], and simulations [136] decoupled the role of water and oxygen in the tribological behavior of MoS_2 in humid environments. It was found that water did not promote MoS_2 oxidation at room temperature. This statement was supported by energy-dispersive X-ray spectroscopy (EDS) analysis in which no oxygen Kα was detected on the worn surface of lubricant films in humid nitrogen environment; i.e., water did not cause the degree of oxidation necessary for detection in this test [131]. This finding is in agreement with Raman spectroscopy results of Windom et al. in which a humid environment had little effect on oxidation compared to dry air or O_2 environments [117]. Moreover, increasing the temperature to values between room temperature and the transition temperature for oxidation greatly improved the tribological properties of the coating [131,133]. This evidence indicates that adsorption/desorption of water is a reversible process, i.e., physisorption rather than chemisorption. Furthermore, ab initio MD simulations modeling the interaction of water with MoS_2 bilayers showed that intercalated water molecules inhibit the sliding motion of both regular and defective layers considerably and that the sliding distance and velocity after a given shear stress are reduced by increasing amounts of water molecules at the interface, consistent with viscous friction behavior [136]. In a recent study, Lee et al. [137] attributed friction enhancement in the presence of intercalated water to the enhancement of phononic energy dissipation at the MoS_2-water interface. It has also been suggested that liquid water could be formed by capillary condensation of vapor in the defects of the MoS_2 crystal structure and that water could then inhibit the easy shear between basal planes [138]; however, no direct observation of adhesion enhancement has yet been reported.

A new interpretation on the role of water in the tribological behavior of MoS_2 was recently proposed by Curry et al. [123]. It was observed that the run-in coefficient of friction for highly-oriented MoS_2 remains the same under dry and humid environments, whereas the run-in behavior is highly environment-dependent in the case of amorphous films. Consequently, it was suggested that water restricted the formation and growth of the shear-induced, highly ordered tribofilms instead of deteriorating the shear strength of existing highly ordered tribofilms. This hypothesis needs further investigation for confirmation.

Recent computational studies [136,142–144] of the energetics and mechanisms of water adsorption and dissociation on MoS_2 films showed that oxidation is much less likely than the simple adsorption of water molecules at edge sites. Additionally, the most favorable locations for the adsorption of water molecules were determined to be Mo edge sites. However, at room temperature, water molecules could dissociate to O and OH that bind to all available edge sites on MoS_2 (i.e., not just Mo) [143]. The higher reactivity of the edges in MoS_2 films emphasizes the potential role of the microstructure in the tribological response of MoS_2 under ambient conditions; the presence of highly ordered structures can significantly improve the tribological behavior of MoS_2 coatings in humid environments [48,123,145–147]. To tailor the microstructure for improving the lubricative properties of MoS_2 under ambient conditions, Chhowalla et al. [148] followed a different approach and generated a thin film of lubricant made of hollow fullerene-like MoS_2 clusters ("onions") using the localized arc discharge method. Ultra-low friction and wear were observed in a humid environment and attributed to the presence of curved S–Mo–S planes that prevented oxidation and preserved the layered structure [148].

Overall, the presence of any environmental contaminant degrades the excellent tribological properties of MoS_2 observed in vacuum. Below the transition temperature for oxidation, water adsorption disrupts the easy-shear properties of MoS_2, whereby oxygen plays only a marginal role in degrading its tribological properties. The adsorption of water is thermodynamically favored, and water diffusion in the bulk has a direct correlation with R.H. and exposure time. As the temperature increases, water species desorb and an improvement in the tribological properties of MoS_2 can be

observed. As the temperature approaches the transition temperature, oxygen-driven, surface-limited oxidation becomes significant and thus, oxidation deteriorates the excellent lubricity of MoS_2 at high temperatures in ambient conditions [131].

At high service temperatures (i.e., above the transition temperature), friction increases with increasing temperature; under ambient conditions this is due to increasing oxidation rates, whereas the thermal dissociation rates of MoS_2 rapidly increase in inert gas or vacuum environments at temperatures above 500 °C [109,118,149,150]. Within this context, the maximum temperature at which MoS_2 provides effective lubrication is highly dependent on (i) the operating environment, e.g., the presence or absence of vacuum and the humidity level, and (ii) the microstructural properties of the MoS_2 coating, including its crystal structure, density, and surface roughness. For instance, in vacuum, the maximum operating temperature of burnished MoS_2 is in the range of 600–700 °C because thermal dissociation of MoS_2 around these temperatures deteriorates its lubricative properties [149]. However, mechanically deposited MoS_2 coatings under ambient conditions could have a maximum operation temperature of 400 °C due to the rapid oxidation of MoS_2 [115,150]. The main challenge therefore is to develop MoS_2 based coatings which can be used over a wide range of operating temperatures.

While the influence of temperature on the tribological properties of MoS_2 under ambient conditions is related to effects associated with the presence of oxygen and water vapor [109,118,149], temperature has also been shown to affect friction and wear under vacuum conditions [151–154] and dry nitrogen environments [155–157]. However, there is disagreement in these reports for the low temperature tribological behavior of MoS_2 (from the cryogenic regime to around −150 °C). Some studies [152,156] reported monotonic increases in friction coefficient with decreasing temperature, while other studies [151,153,155,157] suggested that decreasing the temperature below a certain level does not lead to increasing friction coefficients (Figure 7). At moderate temperatures (up to around 200 °C), the friction, in a thermally activated process, monotonically decreases as temperature increases. Wear rate in this temperature range has been reported to increase as temperature increases, such that the wear rate of an MoS_2 coating doubled as temperature increased from −100 to 100 °C [151]. Curry et al. [154] recently developed a predictive model to correlate the macroscale interfacial shear strength of MoS_2 to temperature, based on the temperature-dependent probabilities for commensurate or incommensurate sliding to occur, taking into account the corresponding energy barriers to sliding. One hypothesis that has emerged from these studies is that the thermally-activated friction behavior is limited to situations where negligible wear takes place, and that the transition from thermally activated friction to athermal friction is a direct result of wear.

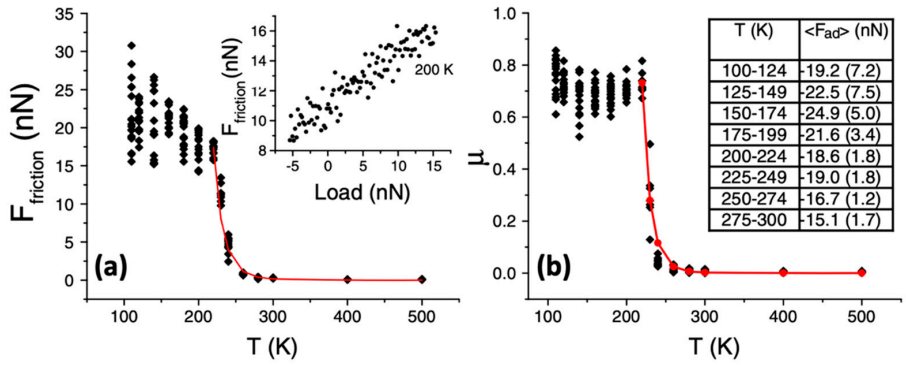

Figure 7. (**a**) Friction force obtained from AFM lateral force measurements at different temperatures for a Si_3N_4 tip sliding over MoS_2. (Inset) Friction-load dependence of this system at T = 200 K; (**b**) Friction coefficients obtained from friction-load plots as a function of temperature. (Inset) Adhesion forces measured at each temperature range. Reprinted with permission from [153], copyright 2009 by the American Physical Society.

Research efforts aimed at achieving MoS_2 solid lubricant coatings that are robust with respect to changes in environment and temperature have primarily used two approaches: (i) changing the

method and parameters of deposition and (ii) adding dopants. First, microstructural properties can be improved by varying the deposition method (such as by using N_2-spray-deposition [123], unbalanced magnetron sputtering [145] or ion-beam-assisted deposition [158]) or parameters (such as lowering the sputter gas pressure [159]) during film preparation to obtain dense films with highly oriented basal planes parallel to the substrate and with the lowest possible density of defects and edge sites. As briefly mentioned above, this approach can improve the environmental resistance of MoS_2 lubricants [123,145–147]. Second, by addition of a small amount of other materials such as metals and inorganic sulfides/oxides, the coating density (and consequently, internal stress), hardness and oxidation resistance can be improved. The effect of dopants on the tribological properties of MoS_2 lubricants is discussed in more detail in Section 6.

To extend the operating range of MoS_2 coatings, adaptive composite coatings have been widely studied. The composite coating improves lubrication not only by the presence of the coating constituents but also by the lubricious products of chemical or physical reactions that happen during sliding. While a comprehensive coverage of the utilization of MoS_2 in composite coatings is not within the scope of this review article, several notable examples will be mentioned here due to their relevance for temperature dependence work. Examples of such adaptive composite coatings include PbO/MoS_2 [55,160], YSZ–Ag–Mo–MoS_2 [161], $Mo_2N/MoS_2/Ag$ [162] and Ag/MoS_2/graphite [163] which extend effective lubrication capabilities over a wide temperature range by combining the lubricity of MoS_2 at lower temperatures and the creation of oxides with easy shear properties at high temperatures [164–166]. However, the chemical reactions are not reversible and the oxides do not provide lubrication at low temperatures, so the ability to withstand thermal cycling is a challenge [167]. One approach is to establish barrier layers to protect some MoS_2 from oxidation [168]. In a different approach to extend the effective lubrication temperature range, Zhang et al. [169] achieved a low friction coefficient (~0.03) and low wear rate (~10−13 mm^3/N·mm) at 300 °C using carbon nanotube (CNT)/MoS_2 composite coatings. These improvements in tribological properties were attributed to an enhancement of mechanical strength due to the high load-bearing capacity of CNTs. Several studies [170,171] showed that diamond-like carbon (DLC) can also be added to the adaptive coating in order to enhance its service temperature range. The DLC phase in these coatings increased hardness and provided a source of carbon for surface graphitization effective for humid environment lubrication. For a detailed description of adaptive coatings designed to improve the temperature range for effective lubrication by MoS_2, readers are referred to [164,172].

6. Structure and Tribological Properties of Doped MoS_2

6.1. Structure of Doped MoS_2

While most studies of structural characterization on doped MoS_2 have focused on synthetic approaches and the effects of doping on electronic structure and catalysis, the obtained results on atomic-scale structure can also be beneficial for the use of doped MoS_2 as a solid lubricant. Here we review the available literature with atomistic characterization of the structures of doped MoS_2, with a focus on bulk rather than monolayers. Experimental characterization of a heterogeneous structure (unlike a single crystal) is quite challenging and, therefore, DFT calculations have played a key role in elucidating structures.

Dopants in MoS_2 can be incorporated in several possible locations. Substitution can occur at either the Mo or S site. Atoms can be added (intercalated) between the MoS_2 layers. They can also be adsorbed at a surface, as adatoms on an MoS_2 sheet (basal plane) or on an edge, which is particularly likely for few-layer MoS_2 or nanosheets. In principle, there could be interstitials within a MoS_2 layer, in the sites within an Mo plane, but there is very limited space and such a structure does not seem to be observed. Adatoms can occur in several high-symmetry sites such as atop Mo, atop S, bridging an Mo-S bond, or in the center of a hexagonal hollow [173]. If an atom is intercalated between two layers in the 2H polytype, these become just two high-symmetry positions: tetrahedrally- or

octahedrally-coordinated [174]. These possible dopant locations in bulk 2H MoS_2 are depicted in Figure 8.

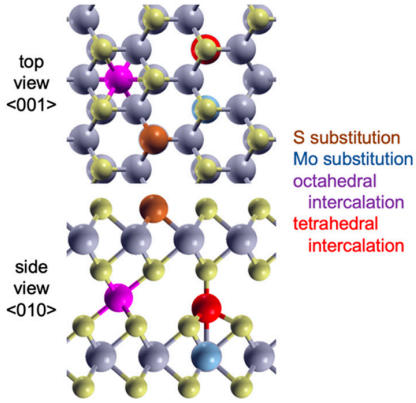

Figure 8. Possible doping sites in 2H MoS_2: substitution at the S site, substitution at the Mo site, octahedral intercalation, and tetrahedral intercalation. Unsubstituted Mo and S are gray and yellow, respectively.

The favorable dopants and their locations can be understood with several considerations [175]. Since MoS_2 formally involves Mo^{4+} and S^{2-} ions, atoms that can adopt a 4^+ oxidation state naturally fit the Mo site, while atoms that can adopt a 2^- oxidation state fit the S site. Intercalated atoms are expected to be neutral. The atom's ionic radius and its compatibility with the Mo or S radii, whether the atom has similar bond length with Mo or S when compared to those in MoS_2, and whether the atom forms a crystal with Mo or S of similar structure to MoS_2 are key points. When these are all similar to MoS_2, alloying in varying proportions may be possible, as is the case for $Mo_{1-x}W_xS_2$, $MoS_{2(1-x)}Se_{2x}$, and $Mo_{1-x}Nb_xS_2$, which have favorable mixing energies and can show substitutional disorder [174,176]. The chemical potentials of Mo, S, and the dopant under synthesis conditions will control which dopant location is favored: for example, S-rich conditions favor Mo substitution [177]. Doping can perturb the local structure (including symmetry breaking and Jahn-Teller distortions) [178,179], alter lattice parameters, or even favor an overall change in crystal structure to a different polytype: Li intercalation causes a change from 2H to 1T [180], and Nb substitution of Mo favors 3R over 2H [181]. Dopants can affect the growth process [182] and the morphology of the resulting crystals or nanostructures, via kinetic or thermodynamic effects [175]. Dopants can be well dispersed or may tend to cluster [177], and in some cases may segregate into competing phases [182,183]. Theoretical studies are complicated by the non-equilibrium conditions in many synthesis approaches, meaning that not only lowest energy structures but also other thermodynamically metastable phases can be formed.

Most doping studies of MoS_2 have used transition metals, which are chemically similar to Mo. DFT calculations for monolayer MoS_2 found that Fe, Mn, W, Cr, V, and Ti dopants substituting for Mo maintain its six-fold coordination, whereas Zn, Au, Ag, Cu, Pt, Pd, Ni, and Co break symmetry and adopt four-fold coordination [178]. A DFT study of Mo substitution on the basal plane surface of the bulk found five-fold coordination for Co, Ni, and Cu, and a six-fold coordination but distorted geometry for Fe; all had shorter M–S bond lengths. Substitution at the edge rather the basal plane was energetically favored [179]. By contrast to the DFT study, experimental results on Zn doping of MoS_2 nanosheets showed little change in Raman or XRD, and were interpreted as Mo substitution without structural distortion [184].

Re can occur naturally in MoS_2. Re substitution of Mo has a low calculated formation energy [27], and it can drive structural changes to 1T or 3R. ReS_2 has a similar structure to MoS_2 although it does have Re-Re bonds in plane [175]; Re doping by a diffusion process resulted in a 1:100 Re:Mo ratio. No Raman changes were observed, and in particular no sign of ReS_2 formation. TEM showed Re in Mo sites, and a small increase in the in-plane lattice spacing, while scanning tunneling microscopy (STM)

suggested Mo substitution within grains and intercalation at grain boundaries [185]. Another STM study also showed Mo substitution by Re [186]. Pt doping has been studied for catalysis. Extended X-ray absorption fine structure (EXAFS) showed Pt–S bonds, indicated Mo substitution, and showed no signs of Pt–Pt bonds, indicating that Pt clusters were not present [178].

Nb doping has been extensively studied since it causes little change in the bonding or electronic structure, which is ideal for electronic doping [177,181]. DFT calculations showed alloying is possible with Nb substituting for Mo up to 25% [174]. Nb has the same oxidation state and a similar ionic radius to Mo, and the NbS_2 phase exists, albeit with a different stacking. DFT shows the octahedral intercalated site is favored over tetrahedral, but Mo substitution is much more favored. There is a local distortion toward the NbS_2 bond lengths [174]. Pairing of Nb dopants in the monolayer is favored by 0.16 eV [177] but only by 0.01 eV in bulk [174]. TEM showed the lattice spacing is preserved and the Raman spectrum showed only subtle changes. Energy-filtered electron transmission microscopy spectrum imaging (EFTEM-SI) showed well dispersed Nb, and EXAFS showed the same atomic environment for Nb and Mo [187]. Interestingly, Nb doping can also induce a transformation from the 2H structure to 3R [181].

Ni doping has been investigated for tribology and catalysis. Sputtering can incorporate 5%–7% concentrations, and it increases the size of acicular (needle-shaped) crystallites [85]. Low concentrations of Ni increase MoS_2 crystal size in hydrothermal synthesis, and change crystallographic orientations. XPS showed the presence of Ni^0 and Ni^{2+}, consistent with intercalation and substitution. High concentrations of Ni cause formation of Ni sulfides instead; Ni_3S_4 was seen in XRD and Raman [182], which is the most stable Ni_xS_y phase according to the Materials Project's calculated phase diagram [22,188]. Another XPS study suggested Ni in nanoclusters is neutral but easily oxidizes in air to Ni^{2+} [28]. Mo substitution is suggested by an XRD/AFM study of 10% doping showing the same structure as undoped material [189]. Co doping is also common for catalysis. Co and Ni in MoS_2 nanoclusters occur as Mo substituents near the edges, changing them from triangular to truncated shapes, which is seen by STM (Figure 9) and predicted by DFT. EXAFS indicates Co and Ni have approximately five bonds to S neighbors, consistent with Mo sites near an edge (or a distorted geometry) [190]. Evidence from EXAFS, STEM (scanning transmission electron microscopy) and DFT for monolayer MoS_2 has shown Co not only in Mo sites but also S sites, and as adatoms in various positions [173].

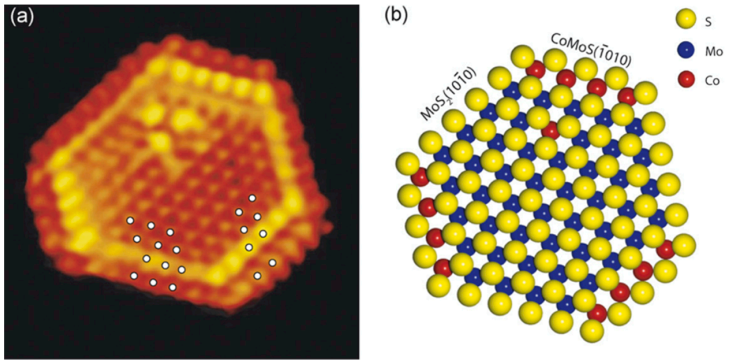

Figure 9. (**a**) Atom-resolved STM image of a Co-doped MoS_2 nanosheet on an Au surface, showing substitution of Mo atoms near edges; (**b**) Ball model. S: yellow, Mo: blue, Co: red. Reprinted from [190] with permission from Elsevier.

Doping with Ti and Zr has been found to distort the structure and reduce crystallinity at high doping levels, related to the octahedral coordination in TiS_2 and ZrS_2. The out-of-plane lattice parameter was not found to change much in XRD. V intercalates and shows expanded layers in XRD, remaining in the 2H polytype. Cr has 2+ and 3+ oxidation states, unlike 4+ for Mo, and therefore causes disordering [175]. Cr doping enhances the MoS_2 longitudinal acoustic band in the Raman

spectrum, with an intensity linear with doping level. Energy-dispersive X-ray spectroscopy (EDX) showed dispersal of Cr throughout flakes, and the elastic modulus was found to be increased [191].

Group VI elements can straightforwardly substitute for S. $MoSe_{2(1-x)}S_{2x}$ alloys are reported to be favorable [176]. $MoS_{2(1-x)}O_{2x}$ (based on MoO_4) has been observed by EXAFS [183] and found to have decreased crystallinity and an expanded interlayer spacing [192]. MoS_xO_{3-x} (based on MoO_3) has been identified through Raman and XPS [193]. Se and Te substitution at 25% causes small systematic changes in lattice parameter. AFM showed the same surface structure for Se, but Te was found to result in surface protrusions [189]. Halogens (F, Cl, Br, I) substituting on the S site have been calculated to have large formation energies, but perhaps substitution could occur by filling S vacancies [177], as suggested by experiments [194]. N doping at the S site has been suggested by XPS, with DFT showing N adopting a "groove" position lower than the S atom plane [195]. Phosphorus is believed to substitute for S, as shown in a laser-doping study of the monolayer, in which sulfur vacancies are created as a first step. The long-term stability of photoluminescence suggested substitution by P rather than surface adsorption as adatoms [196]. H or alkali (Li, K, Cs) atoms can adsorb on MoS_2 and donate electrons, preferring a location atop the Mo site [177]. Li can also intercalate, driving 2H to 1T crystal structure transformations, and large changes in the Raman spectrum; this process can be used in Li-ion batteries [180].

6.2. Tribological Properties of Doped MoS_2

Dopants have been used to improve the tribological properties of MoS_2 coatings for several decades [175]. As discussed in Section 6.1, dopant atoms can exist in layered structures through substitution of atoms in the lattice, at interstitial sites between atoms in the lattice, intercalated between layers, or as a separate phase dispersed in the material. Which of these is observed depends on the dopant and its concentration, as well as the deposition process used to create the coating. Doped coatings are produced using various deposition methods. Sputter deposition, also called sputtering, was one of the earliest techniques and is still commonly used. However, also applied for doped MoS_2 coatings are unbalanced magnetron sputtering, ion beam deposition, and pulsed laser deposition [15]. Dopants that have been studied and shown to improve tribological properties of MoS_2 are Ni, Cr, Ti, Au, Zr, and Sb_2O_3. Doped MoS_2 coatings have been shown to exhibit better tribological properties (i.e., friction, wear and life) than undoped MoS_2 in vacuum, as well as exhibit superior resistance to oxidation which improves performance and storability in air [15].

Understanding the mechanisms by which dopants improve the tribological and oxidation properties of MoS_2 is still a topic of active research. In terms of oxidation resistance, multiple mechanisms have been proposed. First, dopants are thought to affect the growth of MoS_2 crystallites which reduces MoS_2 phase size and in turn increases density [15]. Higher density can improve oxidation resistance by reducing crystalline breakage [197], as well as decreasing the number of edge sites available to oxidize [15]. Dopants are also proposed to passivate edge sites so that they are less reactive with available oxygen [198]. Lastly, in cases where dopants exist as a separate phase, it has been proposed that the dopant atoms bond with oxygen to form an oxide [199].

The beneficial effects of dopants on friction, wear and coating life have also been explained via multiple mechanisms. However, the most widely cited mechanism is increased hardness [65,67,175,200–203]. It has been proposed that hardness increases as a result of distortion of the MoS_2 crystal structure in doped films [65,67]. Hardness directly benefits wear, which is critical for coating life (or endurance) in many applications, including space missions where coatings must function for many years without replacement. Some papers that report improved hardness also observe that dopants can increase the elastic modulus of the coating [201–203]. Hardness has also been associated with increased density (sometimes referred to as reduced porosity) that contributes to improved friction and wear [204,205]. However, increased hardness is not the only mechanism available, and it has been shown that some dopants decrease hardness yet improve performance [198]. For some dopants, the primary mechanism is proposed to be the presence of the dopant as a separate nanoscale phase which imparts beneficial

properties related to the transfer film [200,206,207]. In practice, the mechanism or mechanisms by which a dopant improves coating performance depends on the dopant, its concentration and, to some degree, conditions during coating deposition and operation. For some of the mostly commonly studied dopants, these effects are discussed in more detail below, grouped by proposed mechanism.

Of the dopants believed to improve tribological performance through hardening, Ti has been the most widely studied [65,85,157,198,201,208,209]. It has been proposed that the Ti atoms are either intercalated between MoS_2 layers [67] or substituted with Mo based on observation of a lack of change in crystal c-axis after doping [210]. Ti atoms have been found to be uniformly distributed in the MoS_2 matrix with no Ti-rich clusters or precipitates present [211]. Measurements of 16% Ti coatings showed that the films are slightly sub-stoichiometric in sulfur and amorphous [209]. Ti-doped coatings have been reported to have a columnar platelet structure, with higher concentrations of Ti corresponding to increasing density [212]. Ti has been found to increase coating hardness, but only up to a limiting concentration, after which additional Ti has a detrimental effect [67,212]. Tribological properties also improve with the amount of Ti in the coating, up to a limiting value that has been reported to be 18% [67]. Ti improves oxidation resistance, as verified by measuring the same friction with 10.8% Ti across a range of humidities [212]. Lastly, it was found that Ti-doped MoS_2 performance depends on the counterface material, with ZrO_2 being best among brass, GCr15 steel, WC and ZrO_2 [203].

The hardening mechanism has also been used to explain the beneficial effects of Cr [65,85,198] [208], Zn [65,200], and Ni [85,157,197] dopants to improve friction and wear. The optimum concentration of Cr was found to be 16.6% for hardness and 10% for friction and wear [208]. Zr-doped coatings were found to consist of nanocrystalline Zr in an amorphous matrix and optimum performance was observed at a concentration of 10% [200]. Ni has been shown to improve tribological performance and particularly to mitigate the increase in friction with decreasing temperature that is commonly observed with both MoS_2 and other doped MoS_2 coatings (see Figure 10) [157]. Ni dopants are currently used in several space components [15] because they improve tribological performance at low temperature [157] and are available at more reasonable cost than some of the other metallic dopant options [85]. In general, metal dopants have been shown to increase performance up to some maximum concentration (e.g., 11% [197]), above which the solubility limit is reached, resulting in layering and poor tribological performance [65]. Lastly, doping with Sb_2O_3 [157,197] results in a fine-grained microstructure and a two-phase system with MoS_2 crystallites dispersed in amorphous antimony oxide [197]. The Sb_2O_3-doped coatings were found to have increased density and hardness [205] with an optimum concentration of 35% [197].

The most commonly studied dopant that does not increase hardness is Au [198,201,204,206,207,213]. Unlike Ti, Au-doped MoS_2 consists of domains of nanocrystalline Au particles dispersed in the MoS_2 matrix, where the size of the particles depends on temperature [206,207]. Au dopants have been shown to decrease hardness [198], so tribological improvement is through a different mechanism. It has been proposed that subsurface coarsening of Au nanoparticles provides load support to allow shear of surface MoS_2 basal planes [206]. Direct comparison of MoS_2, Au and Au-doped MoS_2 (at relatively high concentrations >42%) showed the doped coating was superior to both MoS_2 and Au alone. Further, it was reported that the optimal amount of Au was dependent on contact stress, where less Au was better at high stress and more Au was better at low stress [207,213]. To explain this observation, it was hypothesized that, at high stress, Au provided the optimum amount of MoS_2 in the contact, while at low stress more Au limited the amount/size of MoS_2 transferred, providing a thinner, more uniform transfer film [213]. This hypothesis was consistent with the observation that sliding on Au-doped MoS_2 results in the formation of pure, crystalline, aligned MoS_2 about 1 nm thick on the coating (see Figure 11) [206,207].

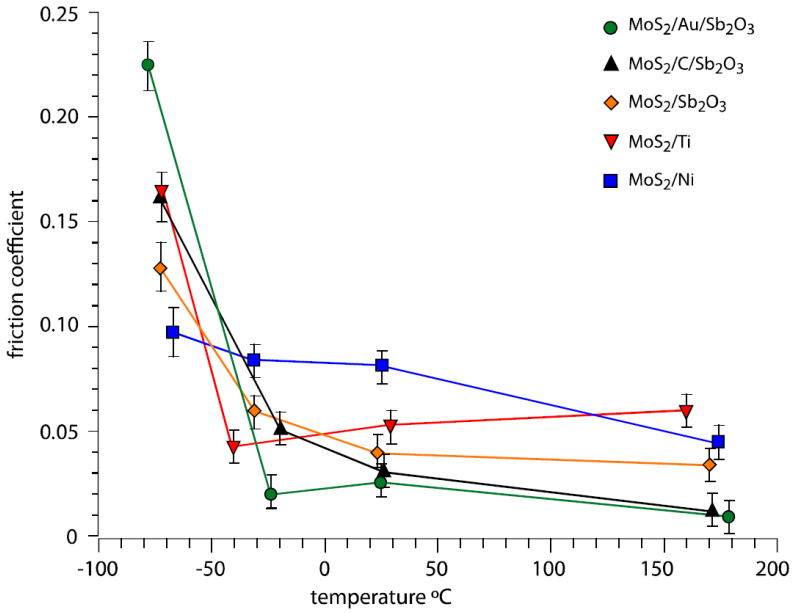

Figure 10. Average friction coefficients as a function of temperature for five different self-mated molybdenum disulfide coatings measured in N_2. Reprinted with permission from [157]. Copyright 2008 Springer Nature.

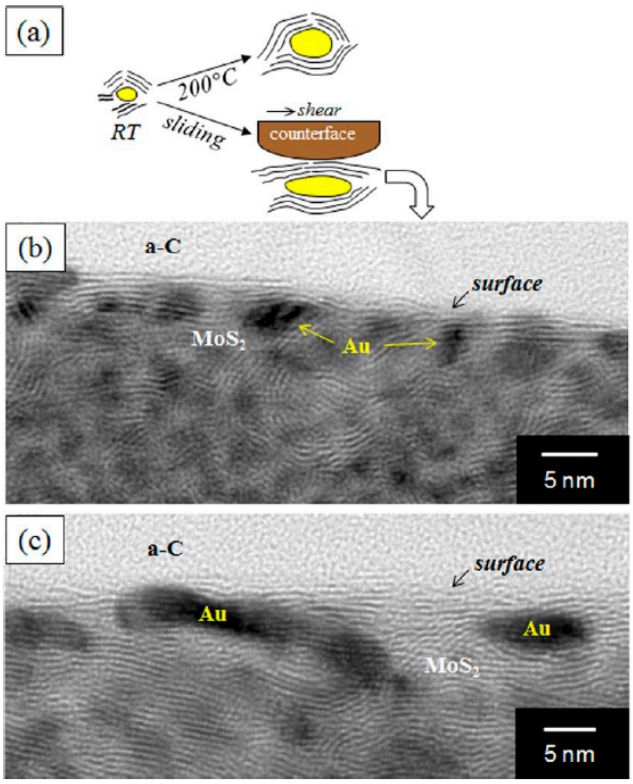

Figure 11. (**a**) Schematic of the contact-stress-dependent behavior of Au-doped MoS_2 coatings supported by cross-section TEM images of coatings after sliding at (**b**) 0.3 and (**c**) 1 GPa. Adapted with permission from [206], copyright 2013 American Chemical Society.

It is also possible to co-dope MoS_2 to leverage the two different mechanisms that are available, to achieve even better tribological performance (particularly in terms of wear resistance). Specifically, Sb_2O_3/Au doped MoS_2 has been frequently studied [157,197,202,214]. For example, coatings with good tribological performance consisted of 11% Sb_2O_3 and 7% Au [214]. Sb_2O_3/Au-doped MoS_2 was found

to have an order of magnitude lower wear rate than Sb_2O_3-doped MoS_2 at room temperature [157]. This feature is particularly important for space applications for which endurance is the most important factor, so Sb_2O_3/Au coatings are currently in use for some space components [15].

Several studies have compared multiple dopants. In measurements of friction and life of Ni, Fe, Au, and Sb_2O_3 doped coatings, all were better than undoped MoS_2 and, among the group, the best was found to be Sb_2O_3/Au [197]. Another comparative study of friction and endurance that included Al, Pt, Ag, W, Cr, Co, Ni, and Ti showed some dopants did not improve performance (Al, Pt, Ag, W) while others had a positive effect (Cr, Co, Ni Ti). For those that improved performance, the optimal metal content was found to be 5%–8% [85]. Another study of metallic dopants showed no difference between the various dopants [65]. In a comparison between Au, Ti, Cr, and WSe_2, the lowest friction and life were exhibited by WSe_2, followed by Au, Ti, and then Cr [198]. Another study focused on temperature dependence measured friction and wear from −80 to 180 °C for Sb_2O_3/Au, Sb_2O_3/C, Sb_2O_3, Ti, and Ni [157]. As shown in Figure 10, they found that Sb_2O_3/Au had the lowest friction above −25 °C, but Ni had the lowest friction at −80 °C. Sb_2O_3/Au exhibited the lowest wear rate at room temperature. An inverse relationship between wear rate and the change in friction coefficient with temperature was also observed, i.e., high room-temperature wear corresponded to smaller increase in friction with decreasing temperature [157]. Opposite trends in friction and wear were observed in another study as well [198]. One challenge with comparison between doped coatings is that different deposition methods may be used for different dopants, which can affect the properties of the resultant coating. One study isolated this parameter by comparing undoped MoS_2, Ti-doped, and Sb_2O_3/Au-doped coatings deposited in the same way [202]. In terms of wear, MoS_2 was best at 30 °C and worst at 100 °C, Sb_2O_3/Au was highly abrasive at 30 °C but performed well at 100 °C, and Ti exhibited good tribological behavior at both temperatures [202].

In summary, dopants have been shown to consistently improve the tribological performance of MoS_2 coatings. There are many different types of dopants, but they can be generally categorized into hard materials (Ti, Ni, Sb_2O_3) and soft materials (Au). In terms of oxidation resistance, the possible roles of these dopants are to densify the film (limiting the number of reactive sites available), passivate edge sites, and sacrificially bond with oxygen. It is possible that all these mechanisms contribute to improved oxidation resistance of doped MoS_2 films. Friction, wear and life of the coatings can also be improved through different mechanisms. However, these mechanisms are highly dependent on the dopant and can be mutually exclusive. Hard materials densify and harden the film, providing direct wear resistance. Soft materials appear to enable formation of thinner and more even MoS_2 films on the surface of the coating, indirectly leading to lower wear. Coatings that contain both hard and soft materials, e.g., Sb_2O_3/Au, may take advantage of both mechanisms. However, a key observation is that wear is often inversely related to friction, particularly friction at low temperatures. Therefore, dopants should be selected based on the priorities of a specific application.

The research performed on doped MoS_2 coatings over the past few decades has clearly demonstrated their great promise. However, as with all new technologies, there are challenges and opportunities. First, scalability is an issue for some deposition techniques [175], which can limit the potential applications for which doped MoS_2 may be considered. Second, not all elements can be used for doping, since doping layered structures with elements that exhibit competing bonding coordination can lead to formation of 3D as opposed to layered structures [175]. Third, and probably most significant, massive amounts of testing will be required before sufficient data are available for doped MoS_2 coatings to be widely used in engineering applications. One limitation to broad testing is that head-to-head comparison of tribological properties is challenging because different coatings are often produced using different deposition techniques and under inconsistent conditions [202]. Testing for a broad range of applications is also hindered by the fact that many of those applications will operate in extreme environments for long durations (e.g., decade-long space missions in vacuum and extreme temperatures); these conditions are difficult to reproduce in a lab setting. Another challenge is lack of availability of doped MoS_2 coatings with controlled composition and deposition. Only a few

research labs have the equipment and experience to produce such materials and, while some coatings (Ni-doped and Sb_2O_3/Au-doped) are commercially available, details about deposition conditions or composition are not usually openly shared. Lastly, given the limitations of experimental testing and the fact that the mechanisms by which these coatings perform their function is hidden from view (i.e., "buried") in sliding interfaces, simulations would be an ideal tool for exploration. However, such simulations require empirical potentials to describe the interatomic interactions and, to model wear, require reactive potentials (which capture bond formation and breaking). At this point, there is no reactive potential available for MoS_2 with commonly used dopants. The development of such a model would enable the direct interrogation of doped MoS_2 sliding mechanisms, which could provide the knowledge base necessary to tune dopants in order to provide optimized tribological properties for specific applications.

7. Conclusions and Outlook

This review provided a focused overview of solid lubrication with MoS_2, starting from the fundamentals of its structure and synthesis, followed by an analysis of the conditions under which its use as a solid lubricant is advantageous, and corresponding tribological applications. The current understanding of the fundamental mechanisms underlying the low friction and wear properties of MoS_2 was discussed in detail, as well as the dependence of these properties on the operating environment and temperature. Finally, the structure and tribological properties of doped MoS_2 were reviewed. The main conclusions of the review and thoughts on emerging research directions are provided below.

There is now agreement regarding the fundamental mechanisms responsible for the lubricative character of MoS_2, namely the ability of its basal planes to orient themselves parallel to the sliding direction during sliding and the low shear strength of the interface between basal planes, facilitating inter-plane sliding with minimal frictional resistance to motion. Despite this general agreement, the conclusions are based mostly on investigating MoS_2 surfaces after the sliding experiments, which does not provide a direct means of studying the details of the dynamic behavior of MoS_2 during sliding. As such, great strides in our understanding of MoS_2 solid lubrication can be made by devising new experimental methods that provide an in situ, high-resolution view of the sliding interface in a MoS_2-lubricated contact. While this would be certainly a long-term goal, such an approach would also provide concrete answers to questions about how wear occurs in MoS_2. Recent cross-sectional TEM work performed on isolated MoS_2 flakes is promising in this regard and future work could build on this achievement to focus on MoS_2 coatings that are more application-oriented.

Research shows that the tribological behavior of MoS_2 is highly sensitive to operating conditions. Based on growing interest in the use of MoS_2 in aerospace/space applications where components are expected to operate in a wide range of temperatures (from the cryogenic to several hundred degrees Celsius) and in different environments, the temperature and environmental dependence of the tribological properties of MoS_2 has been the subject of many studies. In particular, the presence of water or oxygen degrades the excellent lubricative properties of MoS_2 observed in vacuum environments. While some studies show that water adsorption plays an important role in the deterioration of the tribological properties of MoS_2 around room temperature, at higher temperatures oxidation was shown to be responsible for diminishing tribological performance. Generally, in vacuum environment and in the absence of wear, friction has been found to decrease with increasing temperature as predicted for a thermally activated process. Wear rate, however, has been found to increase as the temperature increases. Despite agreement regarding the effect of the operating environment and temperature on the tribological properties of MoS_2, there are still significant discrepancies in the proposed mechanisms, mostly due to difficulties associated with studying different environmental factors (e.g., the presence of water, oxygen or other species) in an isolated fashion as well as design and construction of new experimental setups that would allow extended tests of lubricants at extreme temperatures. Systematic experiments conducted in well-controlled environments, as well as detailed atomistic simulations

employing realistic interaction potentials, can thus provide insight into the structural and chemical changes that occur at the buried sliding interface, which can eventually enable MoS_2 to operate reliably in varying environmental conditions.

The improved tribological performance exhibited by doped MoS_2 coatings when compared with their pristine counterparts (in particular, under challenging environmental conditions) has enabled their use in critical technologies, including, but not limited to those related to space exploration. Despite this fact, significant limitations/challenges remain related to scalability, the range of materials that can be successfully used for doping, and the lack of availability of relevant test setups that can successfully simulate, for instance, decade-long missions under vacuum and at cryogenic temperatures. Moreover, while the specific method of deposition and related parameters are known to affect the tribological performance of doped MoS_2 coatings significantly, systematic studies evaluating these relations do not currently exist, in part due to the fact that details of composition and deposition of commercially successful coatings are not openly shared. Given the experimental difficulties, simulations arise as a viable route for (i) evaluating and understanding the properties of existing doped MoS_2 coatings, especially by studying the buried sliding interface not accessible to conventional experiments, and (ii) predicting new dopants and doping strategies for improved performance. Naturally, the success of such simulations will crucially depend on the availability of accurate, reactive interaction potentials, the development of which could constitute an important direction of research in the near future.

Progress in doped MoS_2 tribology will also benefit from advancement in experimental structural characterization. Standard methods for the analysis of periodic crystals, with diffraction of X-rays, electrons, or neutrons, can provide only limited and average information for heterogeneous structures. Most doping studies have not conclusively identified the structure of the doped materials. More work employing methods that can provide localized information (such as EXAFS and XPS, and high-resolution STM, AFM, and TEM), in conjunction with DFT calculations, is needed to elucidate dopant locations, local environments, and structural distortions. Study of vibrations by Raman and infrared spectroscopy or neutron scattering, supplemented by theoretical studies, are also promising ways to investigate signatures of dopant concentrations and environments. Correlation of detailed structural characterization with tribology studies is needed to identify the structure-property-function relations. Knowledge from the extensive literature on MoS_2 doping for electronic and catalytic applications can also be leveraged to provide new insight and ideas for tribology. Experimental and theoretical work is then needed to better understand how dopants affect growth processes and morphology, and how the resulting structures can be controlled, to target the structures found to be beneficial to tribological performance.

The rapidly widening range of conditions in which mechanical systems and components have to operate efficiently will certainly maintain and accelerate interest in solid lubrication in the near future. Within this context, this review summarized the properties, applications and mechanisms of MoS_2 as a solid lubricant, with the aim of providing a snapshot of our current understanding of this material, as well as inspire future research directions. Focused experimental and computational work are expected to accelerate developments in this field, potentially providing new opportunities for solid lubrication using MoS_2 in applications that traditionally employ oils and greases.

Funding: This research was supported by the Merced nAnomaterials Center for Energy and Sensing (MACES) via the National Aeronautics and Space Administration (NASA) grant no. NNX15AQ01. A.M. and M.R.V. acknowledge support from the National Science Foundation, award # CMMI-1762384.

Conflicts of Interest: The authors declare no conflict of interest.

References

1. Jost, H.P. Tribology—Origin and future. *Wear* **1990**, *136*, 1–17. [CrossRef]
2. Bhushan, B. *Introduction to Tribology*; Wiley: New York, NY, USA, 2013.
3. Holmberg, K.; Erdemir, A. Influence of tribology on global energy consumption, costs and emissions. *Friction* **2017**, *5*, 263–284. [CrossRef]
4. Mang, T.; Bobzin, K.; Bartels, T. *Industrial Tribology: Tribosystems, Friction, Wear and Surface Engineering, Lubrication*; Wiley-VCH: Weinheim, Germany, 2011.
5. Donnet, C.; Erdemir, A. Historical developments and new trends in tribological and solid lubricant coatings. *Surf. Coat. Technol.* **2004**, *180*, 76–84. [CrossRef]
6. Roberts, E.W. Thin solid lubricant films in space. *Tribol. Int.* **1990**, *23*, 95–104. [CrossRef]
7. Roberts, E.W. Space tribology: Its role in spacecraft mechanisms. *J. Phys. D-Appl. Phys.* **2012**, *45*, 503001. [CrossRef]
8. Savan, A.; Pflüger, E.; Voumard, P.; Shröer, A.; Simmonds, M. Modern Solid Lubrication: Recent Developments and Applications of MoS_2. *Lubr. Sci.* **2000**, *12*, 185. [CrossRef]
9. Song, I.; Park, C.; Choi, H.C. Synthesis and properties of molybdenum disulphide: From bulk to atomic layers. *RSC Adv.* **2015**, *5*, 7495–7514. [CrossRef]
10. Koehler, W. Antifriction and Antiabrasive Metal. U.S. Patent 1714564A, 28 May 1929.
11. Donnet, C.; Martin, J.M.; LeMogne, T.; Belin, M. Super-low friction of MoS_2 coatings in various environments. *Tribol. Int.* **1996**, *29*, 123–128. [CrossRef]
12. Winer, W.O. Molybdenum disulfide as a lubricant: A review of the fundamental knowledge. *Wear* **1967**, *10*, 422–452. [CrossRef]
13. Lansdown, A.R. *Molybdenum Disulphide Lubrication*; Elsevier: Amsterdam, The Netherlands, 1999.
14. Voevodin, A.A.; Zabinski, J.S. Nanocomposite and nanostructured tribological materials for space applications. *Compos. Sci. Technol.* **2005**, *65*, 741–748. [CrossRef]
15. Lince, J.R. Doped MoS_2 Coatings and Their Tribology. In *Encyclopedia of Tribology*; Wang, Q.J., Chung, Y.W., Eds.; Springer: Boston, MA, USA, 2013.
16. Novoselov, K.S.; Mishchenko, A.; Carvalho, A.; Castro Neto, A.H. 2D materials and van der Waals heterostructures. *Science* **2016**, *353*, 461. [CrossRef] [PubMed]
17. Peelaers, H.; Van de Walle, C.G. Elastic Constants and Pressure-Induced Effects in MoS_2. *J. Phys. Chem. C* **2014**, *118*, 12073–12076. [CrossRef]
18. Ganatra, R.; Zhang, Q. Few-Layer MoS_2: A Promising Layered Semiconductor. *ACS Nano* **2014**, *8*, 4074–4099. [CrossRef] [PubMed]
19. Hu, T.; Li, R.; Dong, J.M. A new (2 x 1) dimerized structure of monolayer 1T-molybdenum disulfide, studied from first principles calculations. *J. Chem. Phys.* **2013**, *139*, 174702. [CrossRef] [PubMed]
20. Yu, Y.F.; Nam, G.H.; He, Q.Y.; Wu, X.J.; Zhang, K.; Yang, Z.Z.; Chen, J.Z.; Ma, Q.L.; Zhao, M.T.; Liu, Z.Q.; et al. High phase-purity 1T′-MoS_2- and 1T′-$MoSe_2$- layered crystals. *Nat. Chem.* **2018**, *10*, 638–643. [CrossRef] [PubMed]
21. Wypych, F.; Schollhorn, R. 1T-MoS2, a New Metallic Modification of Molybdenum Disulfide. *J. Chem. Soc. -Chem. Commun.* **1992**, *19*, 1386–1388. [CrossRef]
22. Jain, A.; Ong, S.P.; Hautier, G.; Chen, W.; Richards, W.D.; Dacek, S.; Cholia, S.; Gunter, D.; Skinner, D.; Ceder, G.; et al. Commentary: The Materials Project: A materials genome approach to accelerating materials innovation. *APL Mater.* **2013**, *1*, 011002. [CrossRef]
23. Materials Project, mp-2815. Available online: https://materialsproject.org/materials/mp-2815 (accessed on 13 June 2019).
24. Materials Project, mp-1434. Available online: https://materialsproject.org/materials/mp-1434 (accessed on 13 June 2019).
25. Chen, X.B.; Chen, Z.L.; Li, J. Critical electronic structures controlling phase transitions induced by lithium ion intercalation in molybdenum disulphide. *Chin. Sci. Bull.* **2013**, *58*, 1632–1641. [CrossRef]
26. Gaur, A.P.S.; Sahoo, S.; Ahmadi, M.; Dash, S.P.; Guinel, M.J.F.; Katiyar, R.S. Surface Energy Engineering for Tunable Wettability through Controlled Synthesis of MoS_2. *Nano Lett.* **2014**, *14*, 4314–4321. [CrossRef]
27. Komsa, H.P.; Krasheninnikov, A.V. Native defects in bulk and monolayer MoS_2 from first principles. *Phys. Rev. B* **2015**, *91*, 125304. [CrossRef]

28. Escalera-Lopez, D.; Niu, Y.B.; Yin, J.L.; Cooke, K.; Rees, N.V.; Palmer, R.E. Enhancement of the Hydrogen Evolution Reaction from Ni-MoS_2 Hybrid Nanoclusters. *ACS Catal.* **2016**, *6*, 6008–6017. [CrossRef] [PubMed]
29. Ma, X.Y.; Li, J.Q.; An, C.H.; Feng, J.; Chi, Y.H.; Liu, J.X.; Zhang, J.; Sun, Y.G. Ultrathin Co(Ni)-doped MoS_2 nanosheets as catalytic promoters enabling efficient solar hydrogen production. *Nano Res.* **2016**, *9*, 2284–2293. [CrossRef]
30. Feldman, Y.; Wasserman, E.; Srolovitz, D.J.; Tenne, R. High-Rate, Gas-Phase Growth of MoS_2 Nested Inorganic Fullerenes and Nanotubes. *Science* **1995**, *267*, 222–225. [CrossRef] [PubMed]
31. Wang, D.Z.; Zhang, X.Y.; Shen, Y.L.; Wu, Z.Z. Ni-doped MoS_2 nanoparticles as highly active hydrogen evolution electrocatalysts. *RSC Adv.* **2016**, *6*, 16656–16661. [CrossRef]
32. Miki, Y.; Nakazato, D.; Ikuta, H.; Uchida, T.; Wakihara, M. Amorphous MoS_2 as the cathode of lithium secondary batteries. *J. Power Sources* **1995**, *54*, 508–510. [CrossRef]
33. Suzuki, R.; Sakano, M.; Zhang, Y.J.; Akashi, R.; Morikawa, D.; Harasawa, A.; Yaji, K.; Kuroda, K.; Miyamoto, K.; Okuda, T.; et al. Valley-dependent spin polarization in bulk MoS_2 with broken inversion symmetry. *Nat. Nanotechnol.* **2014**, *9*, 611–617. [CrossRef] [PubMed]
34. Jellinek, F.; Brauer, G.; Muller, H. Molybdenum and Niobium Sulphides. *Nature* **1960**, *185*, 376–377. [CrossRef]
35. Geim, A.K.; Novoselov, K.S. The rise of graphene. *Nat. Mater.* **2007**, *6*, 183–191. [CrossRef] [PubMed]
36. Novoselov, K.S.; Jiang, D.; Schedin, F.; Booth, T.J.; Khotkevich, V.V.; Morozov, S.V.; Geim, A.K. Two-dimensional atomic crystals. *Proc. Natl. Acad. Sci. USA* **2005**, *102*, 10451–10453. [CrossRef]
37. Cunningham, G.; Lotya, M.; Cucinotta, C.S.; Sanvito, S.; Bergin, S.D.; Menzel, R.; Shaffer, M.S.P.; Coleman, J.N. Solvent Exfoliation of Transition Metal Dichalcogenides: Dispersibility of Exfoliated Nanosheets Varies Only Weakly between Compounds. *ACS Nano* **2012**, *6*, 3468–3480. [CrossRef] [PubMed]
38. Liu, N.; Kim, P.; Kim, J.H.; Ye, J.H.; Kim, S.; Lee, C.J. Large-Area Atomically Thin MoS_2 Nanosheets Prepared Using Electrochemical Exfoliation. *ACS Nano* **2014**, *8*, 6902–6910. [CrossRef] [PubMed]
39. Zhan, Y.J.; Liu, Z.; Najmaei, S.; Ajayan, P.M.; Lou, J. Large-Area Vapor-Phase Growth and Characterization of MoS_2 Atomic Layers on a SiO_2 Substrate. *Small* **2012**, *8*, 966–971. [CrossRef] [PubMed]
40. Lee, Y.; Lee, J.; Bark, H.; Oh, I.K.; Ryu, G.H.; Lee, Z.; Kim, H.; Cho, J.H.; Ahn, J.H.; Lee, C. Synthesis of wafer-scale uniform molybdenum disulfide films with control over the layer number using a gas phase sulfur precursor. *Nanoscale* **2014**, *6*, 2821–2826. [CrossRef] [PubMed]
41. Lee, Y.H.; Zhang, X.Q.; Zhang, W.J.; Chang, M.T.; Lin, C.T.; Chang, K.D.; Yu, Y.C.; Wang, J.T.W.; Chang, C.S.; Li, L.J.; et al. Synthesis of Large-Area MoS_2 Atomic Layers with Chemical Vapor Deposition. *Adv. Mater.* **2012**, *24*, 2320–2325. [CrossRef] [PubMed]
42. Dumcenco, D.; Ovchinnikov, D.; Marinov, K.; Lazic, P.; Gibertini, M.; Marzari, N.; Sanchez, O.L.; Kung, Y.C.; Krasnozhon, D.; Chen, M.W.; et al. Large-Area Epitaxial Mono layer MoS_2. *ACS Nano* **2015**, *9*, 4611–4620. [CrossRef]
43. Song, I.; Park, C.; Hong, M.; Baik, J.; Shin, H.J.; Choi, H.C. Patternable Large-Scale Molybdenium Disulfide Atomic Layers Grown by Gold-Assisted Chemical Vapor Deposition. *Angew. Chem. Int. Ed.* **2014**, *53*, 1266–1269. [CrossRef] [PubMed]
44. Yu, H.; Liao, M.Z.; Zhao, W.J.; Liu, G.D.; Zhou, X.J.; Wei, Z.; Xu, X.Z.; Liu, K.H.; Hu, Z.H.; Deng, K.; et al. Wafer-Scale Growth and Transfer of Highly-Oriented Monolayer MoS_2 Continuous Films. *ACS Nano* **2017**, *11*, 12001–12007. [CrossRef]
45. George, A.S.; Mutlu, Z.; Ionescu, R.; Wu, R.J.; Jeong, J.S.; Bay, H.H.; Chai, Y.; Mkhoyan, K.A.; Ozkan, M.; Ozkan, C.S. Wafer Scale Synthesis and High Resolution Structural Characterization of Atomically Thin MoS_2 Layers. *Adv. Funct. Mater.* **2014**, *24*, 7461–7466. [CrossRef]
46. Liu, K.K.; Zhang, W.J.; Lee, Y.H.; Lin, Y.C.; Chang, M.T.; Su, C.; Chang, C.S.; Li, H.; Shi, Y.M.; Zhang, H.; et al. Growth of Large-Area and Highly Crystalline MoS_2 Thin Layers on Insulating Substrates. *Nano Lett.* **2012**, *12*, 1538–1544. [CrossRef]
47. Yang, J.; Gu, Y.; Lee, E.; Lee, H.; Park, S.H.; Cho, M.H.; Kim, Y.H.; Kim, H. Wafer-scale synthesis of thickness-controllable MoS_2 films via solution-processing using a dimethylformamide/n-butylamine/2-aminoethanol solvent system. *Nanoscale* **2015**, *7*, 9311–9319. [CrossRef]
48. Fleischauer, P.D. Effects of Crystallite Orientation on Environmental Stability and Lubrication Properties of Sputtered MoS_2 Thin Films. *ASLE Trans.* **1984**, *27*, 82–88. [CrossRef]
49. Martin, J.M.; Donnet, C.; Lemogne, T.; Epicier, T. Superlubricity of Molybdenum Disulfide. *Phys. Rev. B* **1993**, *48*, 10583–10586. [CrossRef] [PubMed]

50. Krause, O.; Muller, F.; Birkmann, S.; Bohm, A.; Ebert, M.; Grozinger, U.; Henning, T.; Hofferbert, R.; Huber, A.; Lemke, D.; et al. High-precision cryogenic wheel mechanisms of the JWST/MIRI instrument: Performance of the flight models. *Proc. SPIE* **2010**, *7739*, 773918. [CrossRef]
51. Spalvins, T. Morphological and frictional behavior of sputtered MoS_2 films. *Thin Solid Films* **1982**, *96*, 17–24. [CrossRef]
52. Bichsel, R.; Buffat, P.; Levy, F. Correlation between process conditions, chemical composition and morphology of MoS_2 films prepared by RF planar magnetron sputtering. *J. Phys. D Appl. Phys.* **1986**, *19*, 1575–1585. [CrossRef]
53. Arslan, E.; Totik, Y.; Efeoglu, I. Comparison of structure and tribological properties of MoS_2-Ti films deposited by biased-dc and pulsed-dc. *Prog. Org. Coat.* **2012**, *74*, 772–776. [CrossRef]
54. Laing, K.; Hampshire, J.; Teer, D.; Chester, G. The effect of ion current density on the adhesion and structure of coatings deposited by magnetron sputter ion plating. *Surf. Coat. Technol.* **1999**, *112*, 177–180. [CrossRef]
55. Zabinski, J.S.; Donley, M.S.; Dyhouse, V.J.; McDevitt, N.T. Chemical and tribological characterization of PbO-MoS_2 films grown by pulsed laser deposition. *Thin Solid Films* **1992**, *214*, 156–163. [CrossRef]
56. Miyoshi, K. *Solid Lubricants and Coatings for Extreme Environments: State-of-the-Art Survey*; NASA/TM: Washington, DC, USA, 2007.
57. Miyoshi, K. Solid Lubricants. In *Encyclopedia of Tribology*; Wang, Q.J., Chung, Y.W., Eds.; Springer: Boston, MA, USA, 2013.
58. Lince, J.R.; Fleischauer, P.D. Solid Lubricants. In *Space Vehicle Mechanisms: Elements of Successful Design*; Conley, P.L., Ed.; Wiley-Interscience: New York, NY, USA, 1998.
59. Chen, Z.; He, X.; Xiao, C.; Kim, S.H. Effect of Humidity on Friction and Wear—A Critical Review. *Lubricants* **2018**, *6*, 74. [CrossRef]
60. Sun, X. Solid Lubricants for Space Mechanisms. In *Encyclopedia of Tribology*; Wang, Q.J., Chung, Y.W., Eds.; Springer: Boston, MA, USA, 2013.
61. Miyoshi, K. Aerospace mechanisms and tribology technology-Case study. *Tribol. Int.* **1999**, *32*, 673–685. [CrossRef]
62. Weidlich, K.; Fischer, M.; Ellenrieder, M.M.; Gross, T.; Salvignol, J.C.; Barho, R.; Neugebauer, C.; Konigsreiter, G.; Trunz, M.; Muller, F.; et al. High-precision cryogenic wheel mechanisms for the JWST NIRSPEC instrument. In Proceedings of the International Conference on Advanced Optical and Mechanical Technologies in Telescopes and Instrumentation, Marseille, France, 23–28 June 2008.
63. Gould, S.G.; Roberts, E.W. The in-vacuo torque performance of dry lubricated ball bearings at cryogenic temperatures. In Proceedings of the 23rd Aerospace Mechanisms Symp., Huntsville, AL, USA, 3–5 May 1989; NASA: Washington, DC, USA, 1989; p. 319.
64. Neugebauer, C.; Supper, L.; Watters, R.; Roberts, E.W.; Demaret, C. Nirspec wheel support mechanism's central duplex bearings cryogenic test results. In Proceedings of the 13th ESMATS, Vienna Austria, 23–25 September 2009.
65. Renevier, N.M.; Fox, V.C.; Teer, D.G.; Hampshire, J. Coating characteristics and tribological properties of sputter-deposited MoS_2/metal composite coatings deposited by closed field unbalanced magnetron sputter ion plating. *Surf. Coat. Technol.* **2000**, *127*, 24–37. [CrossRef]
66. Fox, V.; Jones, A.; Renevier, N.M.; Teer, D.G. Hard lubricating coatings for cutting and forming tools and mechanical components. *Surf. Coat. Technol.* **2000**, *125*, 347–353. [CrossRef]
67. Teer, D.G. New solid lubricant coatings. *Wear* **2001**, *251*, 1068–1074. [CrossRef]
68. Mao, J.; Wang, Y.; Zheng, Z.L.; Deng, D.H. The rise of two-dimensional MoS_2 for catalysis. *Front. Phys.* **2018**, *13*, 138118. [CrossRef]
69. Bernardi, M.; Ataca, C.; Palummo, M.; Grossman, J.C. Optical and Electronic Properties of Two-Dimensional Layered Materials. *Nanophotonics* **2017**, *6*, 479–493. [CrossRef]
70. Martin, J.M.; Pascal, H.; Donnet, C.; Lemogne, T.; Loubet, J.L.; Epicier, T. Superlubricity of MoS_2: Crystal orientation mechanisms. *Surf. Coat. Technol.* **1994**, *68*, 427–432. [CrossRef]
71. Fleischauer, P.D.; Bauer, R. Chemical and Structural Effects on the Lubrication Properties of Sputtered MoS_2 Films. *Tribol. Trans.* **1988**, *31*, 239–250. [CrossRef]
72. Baykara, M.Z.; Vazirisereshk, M.R.; Martini, A. Emerging superlubricity: A review of the state of the art and perspectives on future research. *Appl. Phys. Rev.* **2018**, *5*, 18. [CrossRef]
73. Hirano, M.; Shinjo, K. Atomistic Locking and Friction. *Phys. Rev. B* **1990**, *41*, 11837–11851. [CrossRef]

74. Sokoloff, J.B. Theory of energy dissipation in sliding crystal surfaces. *Phys. Rev. B* **1990**, *42*, 760–765. [CrossRef]
75. Oviedo, J.P.; Santosh, K.C.; Lu, N.; Wang, J.G.; Cho, K.; Wallace, R.M.; Kim, M.J. In Situ TEM Characterization of Shear-Stress-Induced Interlayer Sliding in the Cross Section View of Molybdenum Disulfide. *ACS Nano* **2015**, *9*, 1543–1551. [CrossRef] [PubMed]
76. Li, H.; Wang, J.H.; Gao, S.; Chen, Q.; Peng, L.M.; Liu, K.H.; Wei, X.L. Superlubricity between MoS_2 Monolayers. *Adv. Mater.* **2017**, *29*. [CrossRef]
77. Martin, J.M.; Erdemir, A. Superlubricity: Friction's vanishing act. *Phys. Today* **2018**, *71*, 40–46. [CrossRef]
78. Liu, Y.M.; Song, A.S.; Xu, Z.; Zong, R.L.; Zhang, J.; Yang, W.Y.; Wang, R.; Hu, Y.Z.; Luo, J.B.; Ma, T.B. Interlayer Friction and Superlubricity in Single-Crystalline Contact Enabled by Two-Dimensional Flake-Wrapped Atomic Force Microscope Tips. *ACS Nano* **2018**, *12*, 7638–7646. [CrossRef] [PubMed]
79. Onodera, T.; Morita, Y.; Suzuki, A.; Koyama, M.; Tsuboi, H.; Hatakeyama, N.; Endou, A.; Takaba, H.; Kubo, M.; Dassenoy, F.; et al. A Computational Chemistry Study on Friction of h-MoS_2. Part, I. Mechanism of Single Sheet Lubrication. *J. Phys. Chem. B* **2009**, *113*, 16526–16536. [CrossRef]
80. Onodera, T.; Morita, Y.; Nagumo, R.; Miura, R.; Suzuki, A.; Tsuboi, H.; Hatakeyama, N.; Endou, A.; Takaba, H.; Dassenoy, F.; et al. A Computational Chemistry Study on Friction of h-MoS_2. Part II. Friction Anisotropy. *J. Phys. Chem. B* **2010**, *114*, 15832–15838. [CrossRef] [PubMed]
81. Levita, G.; Cavaleiro, A.; Molinari, E.; Polcar, T.; Righi, M.C. Sliding Properties of MoS_2 Layers: Load and Interlayer Orientation Effects. *J. Phys. Chem. C* **2014**, *118*, 13809–13816. [CrossRef]
82. Ye, Z.J.; Otero-De-La-Roza, A.; Johnson, E.R.; Martini, A. Oscillatory motion in layered materials: Graphene, boron nitride, and molybdenum disulfide. *Nanotechnology* **2015**, *26*, 165701. [CrossRef]
83. Hao, R.; Tedstone, A.A.; Lewis, D.J.; Warrens, C.P.; West, K.R.; Howard, P.; Gaemers, S.; Dillon, S.J.; O'Brien, P. Property Self-Optimization During Wear of MoS_2. *ACS Appl. Mater. Interfaces* **2017**, *9*, 1953–1958. [CrossRef]
84. Tedstone, A.A.; Lewis, D.J.; Hao, R.; Mao, S.M.; Bellon, P.; Averback, R.S.; Warrens, C.P.; West, K.R.; Howard, P.; Gaemers, S.; et al. Mechanical Properties of Molybdenum Disulfide and the Effect of Doping: An in Situ TEM Study. *ACS Appl. Mater. Interfaces* **2015**, *7*, 20829–20834. [CrossRef]
85. Stupp, B.C. Synergistic Effects of Metals Co-Sputtered with MoS_2. *Metall. Prot. Coat.* **1981**, *84*, 257–266. [CrossRef]
86. Deleanu, L.; Cantaragiu, A.; Birsan, I.G.; Podaru, G.; Georgescu, C. Evaluation of the spread range of 3D parameters for coated surfaces. *Tribol. Ind.* **2011**, *33*, 72–78.
87. Horovistiz, A.; Laranjeira, S.; Davim, J.P. 2. Effect of glass fiber reinforcement and the addition of MoS_2 on the tribological behavior of PA66 under dry sliding conditions: A study of distribution of pixel intensity on the counterface. In *Wear of Composite Materials*; De Gruyter: Berlin, Germany, 2018; Volume 9.
88. Soleimani, S.; Sukumaran, J.; Kumcu, A.; De Baets, P.; Philips, W. Quantifying abrasion and micro-pits in polymer wear using image processing techniques. *Wear* **2014**, *319*, 123–137. [CrossRef]
89. Binnig, G.; Quate, C.F.; Gerber, C. Atomic Force Microscope. *Phys. Rev. Lett.* **1986**, *56*, 930–933. [CrossRef]
90. Mate, C.M.; McClelland, G.M.; Erlandsson, R.; Chiang, S. Atomic-scale Friction of a Tungsten Tip on a Graphite Surface. *Phys. Rev. Lett.* **1987**, *59*, 1942–1945. [CrossRef]
91. Novoselov, K.S.; Geim, A.K.; Morozov, S.V.; Jiang, D.; Zhang, Y.; Dubonos, S.V.; Grigorieva, I.V.; Firsov, A.A. Electric field effect in atomically thin carbon films. *Science* **2004**, *306*, 666–669. [CrossRef]
92. Spear, J.C.; Ewers, B.W.; Batteas, J.D. 2D-nanomaterials for controlling friction and wear at interfaces. *Nano Today* **2015**, *10*, 301–314. [CrossRef]
93. Schumacher, A.; Kruse, N.; Prins, R.; Meyer, E.; Lüthi, R.; Howald, L.; Güntherodt, H.J.; Scandella, L. Influence of humidity on friction measurements of supported MoS_2 single layers. *J. Vac. Sci. Technol. B Microelectron. Nanometer Struct. Process. Meas. Phenom.* **1996**, *14*, 1264–1267. [CrossRef]
94. Lee, C.; Li, Q.Y.; Kalb, W.; Liu, X.Z.; Berger, H.; Carpick, R.W.; Hone, J. Frictional Characteristics of Atomically Thin Sheets. *Science* **2010**, *328*, 76–80. [CrossRef]
95. Filleter, T.; McChesney, J.L.; Bostwick, A.; Rotenberg, E.; Emtsev, K.V.; Seyller, T.; Horn, K.; Bennewitz, R. Friction and Dissipation in Epitaxial Graphene Films. *Phys. Rev. Lett.* **2009**, *102*, 086102. [CrossRef]
96. Ye, Z.J.; Balkanci, A.; Martini, A.; Baykara, M.Z. Effect of roughness on the layer-dependent friction of few-layer graphene. *Phys. Rev. B* **2017**, *96*, 115401. [CrossRef]

97. Lavini, F.; Calo, A.; Gao, Y.; Albisetti, E.; Li, T.D.; Cao, T.F.; Li, G.Q.; Cao, L.Y.; Aruta, C.; Riedo, E. Friction and work function oscillatory behavior for an even and odd number of layers in polycrystalline MoS_2. *Nanoscale* **2018**, *10*, 8304–8312. [CrossRef] [PubMed]
98. Fang, L.; Liu, D.M.; Guo, Y.Z.; Liao, Z.M.; Luo, J.B.; Wen, S.Z. Thickness dependent friction on few-layer MoS_2, WS_2, and WSe_2. *Nanotechnology* **2017**, *28*, 245703. [CrossRef] [PubMed]
99. Cao, X.A.; Gan, X.H.; Lang, H.J.; Yu, K.; Ding, S.Y.; Peng, Y.T.; Yi, W.M. Anisotropic nanofriction on MoS_2 with different thicknesses. *Tribol. Int.* **2019**, *134*, 308–316. [CrossRef]
100. Choi, J.S.; Kim, J.S.; Byun, I.S.; Lee, D.H.; Lee, M.J.; Park, B.H.; Lee, C.; Yoon, D.; Cheong, H.; Lee, K.H.; et al. Friction Anisotropy-Driven Domain Imaging on Exfoliated Monolayer Graphene. *Science* **2011**, *333*, 607–610. [CrossRef] [PubMed]
101. Cho, D.H.; Jung, J.; Kim, C.; Lee, J.; Oh, S.D.; Kim, K.S.; Lee, C. Comparison of Frictional Properties of CVD-Grown MoS_2 and Graphene Films under Dry Sliding Conditions. *Nanomaterials* **2019**, *9*, 293. [CrossRef] [PubMed]
102. Vazirisereshk, M.R.; Ye, H.; Ye, Z.; Otero-de-la-Roza, A.; Zhao, M.; Gao, Z.; Johnson, A.T.C.; Johnson, E.R.; Carpick, R.W.; Martini, A. Origin of Nanoscale Friction Contrast between Supported Graphene, MoS_2, and a Graphene/MoS_2 Heterostructure. *Nano Lett.* **2019**. under review.
103. Peterson, M.B.; Johnson, R.L. *Friction and Wear Investigation of Molybdenum Disulfide 1: Effect of Moisture*; Technical Note 3055; NACA: Washington, DC, USA, 1953.
104. Ross, S.; Sussman, A. Surface Oxidation of Molybdenum Disulfide. *J. Phys. Chem.* **1955**, *59*, 889–892. [CrossRef]
105. Haltner, A.J.; Oliver, C.S. Effect of Water Vapor on Friction of Molybdenum Disulfide. *Ind. Eng. Chem. Fundam.* **1966**, *5*, 348–355. [CrossRef]
106. Pardee, R.P. The Effect of Humidity on Low-Load Frictional Properties of a Bonded Solid Film Lubricant. *ASLE Trans.* **1972**, *15*, 130–142. [CrossRef]
107. Panitz, J.K.G.; Pope, L.E.; Lyons, J.E.; Staley, D.J. The tribological properties of MoS_2 coatings in vacuum, low relative humidity, and high relative humidity environments. *J. Vac. Sci. Technol. A* **1988**, *6*, 1166–1170. [CrossRef]
108. Tagawa, M.; Yokota, K.; Ohmae, N.; Matsumoto, K.; Suzuki, M. Hyperthermal Atomic Oxygen Interaction with MoS_2 Lubricants Relevance to Space Environmental Effects in Low Earth Orbit—Atomic Oxygen-Induced Oxidation. *Tribol. Lett.* **2004**, *17*, 859–865. [CrossRef]
109. Khare, H.S.; Burris, D.L. The Effects of Environmental Water and Oxygen on the Temperature-Dependent Friction of Sputtered Molybdenum Disulfide. *Tribol. Lett.* **2013**, *52*, 485–493. [CrossRef]
110. Tagawa, M.; Ikeda, J.; Kinoshita, H.; Umeno, M.; Ohmae, N. Effect of Atomic Oxygen Exposures on the Tribological Properties of Molybdenum Disulfide Lubricants. In *Protection of Space Materials from the Space Environment*; Springer: Dordrecht, The Netherlands, 2001; pp. 73–84.
111. Miyoshi, K. *Solid Lubrication Fundamentals and Applications*; CRC Press: Boca Raton, FL, USA, 2001.
112. Liang, T.; Sawyer, W.G.; Perry, S.S.; Sinnott, S.B.; Phillpot, S.R. Energetics of Oxidation in MoS_2 Nanoparticles by Density Functional Theory. *J. Phys. Chem. C* **2011**, *115*, 10606–10616. [CrossRef]
113. Johnson, M.R. The Galileo High Gain Antenna Deployment Anomaly. In Proceedings of the 28th Aerospace Mechanisms Symposium, NASA Lewis Research Center, Cleveland, OH, USA, 18–20 May 1994; pp. 359–377.
114. Fusaro, R.L. *Lubrication and Failure Mechanisms of Molybdenum Disulfide Films I-Effect of Atmosphere*; Technical Note 1343; NASA: Washington, DC, USA, 1978.
115. Muratore, C.; Bultman, J.E.; Aouadi, S.M.; Voevodin, A.A. In situ Raman spectroscopy for examination of high temperature tribological processes. *Wear* **2011**, *270*, 140–145. [CrossRef]
116. Spychalski, W.L.; Pisarek, M.; Szoszkiewicz, R. Microscale Insight into Oxidation of Single MoS_2 Crystals in Air. *J. Phys. Chem. C* **2017**, *121*, 26027–26033. [CrossRef]
117. Windom, B.C.; Sawyer, W.G.; Hahn, D.W. A Raman Spectroscopic Study of MoS_2 and MoO_3: Applications to Tribological Systems. *Tribol. Lett.* **2011**, *42*, 301–310. [CrossRef]
118. Kubart, T.; Polcar, T.; Kopecký, L.; Novák, R.; Nováková, D. Temperature dependence of tribological properties of MoS_2 and $MoSe_2$ coatings. *Surf. Coat. Technol.* **2005**, *193*, 230–233. [CrossRef]
119. Sliney, H.E. *High Temperature Solid Lubricants: When and Where to Use Them*; Technical Memorandum 68201; NASA: Washington, DC, USA, 1973.

120. Yamamoto, M.; Einstein, T.L.; Fuhrer, M.S.; Cullen, W.G. Anisotropic Etching of Atomically Thin MoS_2. *J. Phys. Chem. C* **2013**, *117*, 25643–25649. [CrossRef]
121. Zhang, X.; Qiao, L.; Chai, L.; Xu, J.; Shi, L.; Wang, P. Structural, mechanical and tribological properties of Mo–S–N solid lubricant films. *Surf. Coat. Technol.* **2016**, *296*, 185–191. [CrossRef]
122. Wang, P.; Qiao, L.; Xu, J.; Li, W.; Liu, W. Erosion Mechanism of MoS_2-Based Films Exposed to Atomic Oxygen Environments. *ACS Appl. Mater. Interfaces* **2015**, *7*, 12943–12950. [CrossRef] [PubMed]
123. Curry, J.F.; Argibay, N.; Babuska, T.; Nation, B.; Martini, A.; Strandwitz, N.C.; Dugger, M.T.; Krick, B.A. Highly Oriented MoS_2 Coatings: Tribology and Environmental Stability. *Tribol. Lett.* **2016**, *64*, 11. [CrossRef]
124. Curry, J.F.; Wilson, M.A.; Luftman, H.S.; Strandwitz, N.C.; Argibay, N.; Chandross, M.; Sidebottom, M.A.; Krick, B.A. Impact of Microstructure on MoS_2 Oxidation and Friction. *ACS Appl. Mater. Interfaces* **2017**, *9*, 28019–28026. [CrossRef] [PubMed]
125. Gao, X.; Fu, Y.; Jiang, D.; Wang, D.; Weng, L.; Yang, J.; Sun, J.; Hu, M. Responses of TMDs-metals composite films to atomic oxygen exposure. *J. Alloy. Compd.* **2018**, *765*, 854–861. [CrossRef]
126. Tagawa, M.; Yokota, K.; Ochi, K.; Akiyama, M.; Matsumoto, K.; Suzuki, M. Comparison of Macro and Microtribological Property of Molybdenum Disulfide Film Exposed to LEO Space Environment. *Tribol. Lett.* **2012**, *45*, 349–356. [CrossRef]
127. Tagawa, M.; Muromoto, M.; Hachiue, S.; Yokota, K.; Ohmae, N.; Matsumoto, K.; Suzuki, M. Hyperthermal atomic oxygen interaction with MoS_2 lubricants and relevance to space environmental effects in low earth orbit–effects on friction coefficient and wear-life. *Tribol. Lett.* **2005**, *18*, 437–443. [CrossRef]
128. Wei, R.; Wilbur, P.J.; Buchholz, B.W.; Kustas, F.M. In Situ Tribological Evaluation of Greases and Solid Lubricants in a Simulated Atomic Oxygen Environment. *Tribol. Trans.* **1995**, *38*, 950–958. [CrossRef]
129. Gao, X.; Hu, M.; Sun, J.; Fu, Y.; Yang, J.; Liu, W.; Weng, L. Changes in the composition, structure and friction property of sputtered MoS_2 films by LEO environment exposure. *Appl. Surf. Sci.* **2015**, *330*, 30–38. [CrossRef]
130. Tagawa, M.; Yokota, K.; Matsumoto, K.; Suzuki, M.; Teraoka, Y.; Kitamura, A.; Belin, M.; Fontaine, J.; Martin, J.M. Space environmental effects on MoS_2 and diamond-like carbon lubricating films: Atomic oxygen-induced erosion and its effect on tribological properties. *Surf. Coat. Technol.* **2007**, *202*, 1003–1010. [CrossRef]
131. Khare, H.S.; Burris, D.L. Surface and Subsurface Contributions of Oxidation and Moisture to Room Temperature Friction of Molybdenum Disulfide. *Tribol. Lett.* **2014**, *53*, 329–336. [CrossRef]
132. Stewart, T.B.; Fleischauer, P.D. Chemistry of sputtered molybdenum disulfide films. *Inorg. Chem.* **1982**, *21*, 2426–2431. [CrossRef]
133. Serpini, E.; Rota, A.; Ballestrazzi, A.; Marchetto, D.; Gualtieri, E.; Valeri, S. The role of humidity and oxygen on MoS_2 thin films deposited by RF PVD magnetron sputtering. *Surf. Coat. Technol.* **2017**, *319*, 345–352. [CrossRef]
134. Pritchard, C.; Midgley, J.W. The effect of humidity on the friction and life of unbonded molybdenum disulphide films. *Wear* **1969**, *13*, 39–50. [CrossRef]
135. Johnston, R.R.M.; Moore, A.J.W. Water Adsorption on Molybdenum Disulfide Containing Surface Contaminants. *J. Phys. Chem.* **1964**, *68*, 3399–3406. [CrossRef]
136. Levita, G.; Righi, M.C. Effects of Water Intercalation and Tribochemistry on MoS_2 Lubricity: An Ab Initio Molecular Dynamics Investigation. *Chem. Phys. Chem.* **2017**, *18*, 1475–1480. [CrossRef] [PubMed]
137. Lee, H.; Jeong, H.; Suh, J.; Doh, W.H.; Baik, J.; Shin, H.J.; Ko, J.H.; Wu, J.; Kim, Y.H.; Park, J.Y. Nanoscale Friction on Confined Water Layers Intercalated between MoS_2 Flakes and Silica. *J. Phys. Chem. C* **2019**, *123*, 8827–8835. [CrossRef]
138. Uemura, M.; Saito, K.; Nakao, K. A Mechanism of Vapor Effect on Friction Coefficient of Molybdenum Disulfide. *Tribol. Trans.* **1990**, *33*, 551–556. [CrossRef]
139. Lancaster, J.K. A review of the influence of environmental humidity and water on friction, lubrication and wear. *Tribol. Int.* **1990**, *23*, 371–389. [CrossRef]
140. Holinski, R.; Gänsheimer, J. A study of the lubricating mechanism of molybdenum disulfide. *Wear* **1972**, *19*, 329–342. [CrossRef]
141. Zhao, X.; Perry, S.S. The Role of Water in Modifying Friction within MoS_2 Sliding Interfaces. *ACS Appl. Mater. Interfaces* **2010**, *2*, 1444–1448. [CrossRef]
142. Ataca, C.; Ciraci, S. Dissociation of H_2O at the vacancies of single-layer MoS_2. *Phys. Rev. B* **2012**, *85*, 195410. [CrossRef]

143. Ghuman, K.K.; Yadav, S.; Singh, C.V. Adsorption and Dissociation of H_2O on Monolayered MoS_2 Edges: Energetics and Mechanism from ab Initio Simulations. *J. Phys. Chem. C* **2015**, *119*, 6518–6529. [CrossRef]
144. Levita, G.; Restuccia, P.; Righi, M.C. Graphene and MoS_2 interacting with water: A comparison by ab initio calculations. *Carbon* **2016**, *107*, 878–884. [CrossRef]
145. Vierneusel, B.; Schneider, T.; Tremmel, S.; Wartzack, S.; Gradt, T. Humidity resistant MoS_2 coatings deposited by unbalanced magnetron sputtering. *Surf. Coat. Technol.* **2013**, *235*, 97–107. [CrossRef]
146. Muratore, C.; Voevodin, A.A. Control of molybdenum disulfide basal plane orientation during coating growth in pulsed magnetron sputtering discharges. *Thin Solid Films* **2009**, *517*, 5605–5610. [CrossRef]
147. Gradt, T.; Schneider, T. Tribological Performance of MoS_2 Coatings in Various Environments. *Lubricants* **2016**, *4*, 32. [CrossRef]
148. Chhowalla, M.; Amaratunga, G.A.J. Thin films of fullerene-like MoS_2 nanoparticles with ultra-low friction and wear. *Nature* **2000**, *407*, 164. [CrossRef]
149. Kohli, A.K.; Prakash, B. Contact Pressure Dependency in Frictional Behavior of Burnished Molybdenum Disulphide Coatings. *Tribol. Trans.* **2001**, *44*, 147–151. [CrossRef]
150. Sliney, H.E. Solid lubricant materials for high temperatures—A review. *Tribol. Int.* **1982**, *15*, 303–315. [CrossRef]
151. Colbert, R.S.; Sawyer, W.G. Thermal dependence of the wear of molybdenum disulphide coatings. *Wear* **2010**, *269*, 719–723. [CrossRef]
152. Dunckle, C.G.; Aggleton, M.; Glassman, J.; Taborek, P. Friction of molybdenum disulfide–titanium films under cryogenic vacuum conditions. *Tribol. Int.* **2011**, *44*, 1819–1826. [CrossRef]
153. Zhao, X.; Phillpot, S.R.; Sawyer, W.G.; Sinnott, S.B.; Perry, S.S. Transition from Thermal to Athermal Friction under Cryogenic Conditions. *Phys. Rev. Lett.* **2009**, *102*, 186102. [CrossRef] [PubMed]
154. Curry, J.F.; Hinkle, A.R.; Babuska, T.F.; Wilson, M.A.; Dugger, M.T.; Krick, B.A.; Argibay, N.; Chandross, M. Atomistic Origins of Temperature-Dependent Shear Strength in 2D Materials. *ACS Appl. Nano Mater.* **2018**, *1*, 5401–5407. [CrossRef]
155. Curry, J.F.; Babuska, T.F.; Brumbach, M.T.; Argibay, N. Temperature-Dependent Friction and Wear of MoS_2/Sb2O3/Au Nanocomposites. *Tribol. Lett.* **2016**, *64*, 18. [CrossRef]
156. Babuska, T.F.; Pitenis, A.A.; Jones, M.R.; Nation, B.L.; Sawyer, W.G.; Argibay, N. Temperature-Dependent Friction and Wear Behavior of PTFE and MoS_2. *Tribol. Lett.* **2016**, *63*, 15. [CrossRef]
157. Hamilton, M.A.; Alvarez, L.A.; Mauntler, N.A.; Argibay, N.; Colbert, R.; Burris, D.L.; Muratore, C.; Voevodin, A.A.; Perry, S.S.; Sawyer, W.G. A Possible Link Between Macroscopic Wear and Temperature Dependent Friction Behaviors of MoS_2 Coatings. *Tribol. Lett.* **2008**, *32*, 91–98. [CrossRef]
158. Seitzman, L.E.; Bolster, R.N.; Singer, I.L. Effects of temperature and ion-to-atom ratio on the orientation of IBAD MoS_2 coatings. *Thin Solid Films* **1995**, *260*, 143–147. [CrossRef]
159. Moser, J.; Lévy, F.; Bussy, F. Composition and growth mode of MoSx sputtered films. *J. Vac. Sci. Technol. A* **1994**, *12*, 494–500. [CrossRef]
160. Zabinski, J.S.; Day, A.E.; Donley, M.S.; Dellacorte, C.; McDevitt, N.T. Synthesis and characterization of a high-temperature oxide lubricant. *J. Mater. Sci.* **1994**, *29*, 5875–5879. [CrossRef]
161. Muratore, C.; Voevodin, A.A. Molybdenum disulfide as a lubricant and catalyst in adaptive nanocomposite coatings. *Surf. Coat. Technol.* **2006**, *201*, 4125–4130. [CrossRef]
162. Aouadi, S.M.; Paudel, Y.; Simonson, W.J.; Ge, Q.; Kohli, P.; Muratore, C.; Voevodin, A.A. Tribological investigation of adaptive Mo_2N/MoS_2/Ag coatings with high sulfur content. *Surf. Coat. Technol.* **2009**, *203*, 1304–1309. [CrossRef]
163. Chen, F.; Feng, Y.; Shao, H.; Zhang, X.; Chen, J.; Chen, N. Friction and Wear Behaviors of Ag/MoS_2/G Composite in Different Atmospheres and at Different Temperatures. *Tribol. Lett.* **2012**, *47*, 139–148. [CrossRef]
164. Voevodin, A.A.; Muratore, C.; Aouadi, S.M. Hard coatings with high temperature adaptive lubrication and contact thermal management: Review. *Surf. Coat. Technol.* **2014**, *257*, 247–265. [CrossRef]
165. Yang, J.-F.; Jiang, Y.; Hardell, J.; Prakash, B.; Fang, Q.-F. Influence of service temperature on tribological characteristics of self-lubricant coatings: A review. *Front. Mater. Sci.* **2013**, *7*, 28–39. [CrossRef]
166. Aouadi, S.M.; Gao, H.; Martini, A.; Scharf, T.W.; Muratore, C. Lubricious oxide coatings for extreme temperature applications: A review. *Surf. Coat. Technol.* **2014**, *257*, 266–277. [CrossRef]

167. Aouadi, S.M.; Luster, B.; Kohli, P.; Muratore, C.; Voevodin, A.A. Progress in the development of adaptive nitride-based coatings for high temperature tribological applications. *Surf. Coat. Technol.* **2009**, *204*, 962–968. [CrossRef]
168. Muratore, C.; Voevodin, A.A. Chameleon Coatings: Adaptive Surfaces to Reduce Friction and Wear in Extreme Environments. *Annu. Rev. Mater. Res.* **2009**, *39*, 297–324. [CrossRef]
169. Zhang, X.; Luster, B.; Church, A.; Muratore, C.; Voevodin, A.A.; Kohli, P.; Aouadi, S.; Talapatra, S. Carbon Nanotube−MoS_2 Composites as Solid Lubricants. *ACS Appl. Mater. Interfaces* **2009**, *1*, 735–739. [CrossRef]
170. Voevodin, A.A.; Fitz, T.A.; Hu, J.J.; Zabinski, J.S. Nanocomposite tribological coatings with "chameleon" surface adaptation. *J. Vac. Sci. Technol. A* **2002**, *20*, 1434–1444. [CrossRef]
171. Baker, C.C.; Chromik, R.R.; Wahl, K.J.; Hu, J.J.; Voevodin, A.A. Preparation of chameleon coatings for space and ambient environments. *Thin Solid Films* **2007**, *515*, 6737–6743. [CrossRef]
172. Torres, H.; Rodríguez Ripoll, M.; Prakash, B. Tribological behaviour of self-lubricating materials at high temperatures. *Int. Mater. Rev.* **2018**, *63*, 309–340. [CrossRef]
173. Liu, G.L.; Robertson, A.W.; Li, M.M.J.; Kuo, W.C.H.; Darby, M.T.; Muhieddine, M.H.; Lin, Y.C.; Suenaga, K.; Stamatakis, M.; Warner, J.H.; et al. MoS_2 monolayer catalyst doped with isolated Co atoms for the hydrodeoxygenation reaction. *Nat. Chem.* **2017**, *9*, 810–816. [CrossRef] [PubMed]
174. Ivanovskaya, V.V.; Zobelli, A.; Gloter, A.; Brun, N.; Serin, V.; Colliex, C. Ab initio study of bilateral doping within the MoS_2-NbS_2 system. *Phys. Rev. B* **2008**, *78*, 134104. [CrossRef]
175. Tedstone, A.A.; Lewis, D.J.; O'Brien, P. Synthesis, Properties, and Applications of Transition Metal-Doped Layered Transition Metal Dichalcogenides. *Chem. Mater.* **2016**, *28*, 1965–1974. [CrossRef]
176. Kutana, A.; Penev, E.S.; Yakobson, B.I. Engineering electronic properties of layered transition-metal dichalcogenide compounds through alloying. *Nanoscale* **2014**, *6*, 5820–5825. [CrossRef] [PubMed]
177. Dolui, K.; Rungger, I.; Das Pemmaraju, C.; Sanvito, S. Possible doping strategies for MoS_2 monolayers: An ab initio study. *Phys. Rev. B* **2013**, *88*, 075420. [CrossRef]
178. Deng, J.; Li, H.B.; Xiao, J.P.; Tu, Y.C.; Deng, D.H.; Yang, H.X.; Tian, H.F.; Li, J.Q.; Ren, P.J.; Bao, X.H. Triggering the electrocatalytic hydrogen evolution activity of the inert two-dimensional MoS_2 surface via single-atom metal doping. *Energy Environ. Sci.* **2015**, *8*, 1594–1601. [CrossRef]
179. Hakala, M.; Kronberg, R.; Laasonen, K. Hydrogen adsorption on doped MoS_2 nanostructures. *Sci. Rep.* **2017**, *7*, 15243. [CrossRef]
180. Benavente, E.; Santa Ana, M.A.; Mendizabal, F.; Gonzalez, G. Intercalation chemistry of molybdenum disulfide. *Coord. Chem. Rev.* **2002**, *224*, 87–109. [CrossRef]
181. Suh, J.; Tan, T.L.; Zhao, W.J.; Park, J.; Lin, D.Y.; Park, T.E.; Kim, J.; Jin, C.H.; Saigal, N.; Ghosh, S.; et al. Reconfiguring crystal and electronic structures of MoS_2 by substitutional doping. *Nat. Commun.* **2018**, *9*, 199. [CrossRef]
182. Kondekar, N.; Boebinger, M.G.; Tian, M.; Kirmani, M.H.; McDowell, M.T. The Effect of Nickel on MoS_2 Growth Revealed with in Situ Transmission Electron Microscopy. *ACS Nano* **2019**. [CrossRef] [PubMed]
183. Lince, J.R.; Hilton, M.R.; Bommannavar, A.S. Metal incorporation in sputter-deposited MoS_2 films studied by extended x-ray absorption fine structure. *J. Mater. Res.* **1995**, *10*, 2091–2105. [CrossRef]
184. Shi, Y.; Zhou, Y.; Yang, D.R.; Xu, W.X.; Wang, C.; Wang, F.B.; Xu, J.J.; Xia, X.H.; Chen, H.Y. Energy Level Engineering of MoS_2 by Transition-Metal Doping for Accelerating Hydrogen Evolution Reaction. *J. Am. Chem. Soc.* **2017**, *139*, 15479–15485. [CrossRef] [PubMed]
185. Hallam, T.; Monaghan, S.; Gity, F.; Ansari, L.; Schmidt, M.; Downing, C.; Cullen, C.P.; Nicolosi, V.; Hurley, P.K.; Duesberg, G.S. Rhenium-doped MoS_2 films. *Appl. Phys. Lett.* **2017**, *111*, 203101. [CrossRef]
186. Lin, Y.C.; Dumcenco, D.O.; Komsa, H.P.; Niimi, Y.; Krasheninnikov, A.V.; Huang, Y.S.; Suenaga, K. Properties of Individual Dopant Atoms in Single-Layer MoS_2: Atomic Structure, Migration, and Enhanced Reactivity. *Adv. Mater.* **2014**, *26*, 2857–2861. [CrossRef] [PubMed]
187. Suh, J.; Park, T.E.; Lin, D.Y.; Fu, D.Y.; Park, J.; Jung, H.J.; Chen, Y.B.; Ko, C.; Jang, C.; Sun, Y.H.; et al. Doping against the Native Propensity of MoS_2: Degenerate Hole Doping by Cation Substitution. *Nano Lett.* **2014**, *14*, 6976–6982. [CrossRef] [PubMed]
188. Jain, A.; Hautier, G.; Ong, S.P.; Moore, C.J.; Fischer, C.C.; Persson, K.A.; Ceder, G. Formation enthalpies by mixing GGA and GGA plus U calculations. *Phys. Rev. B* **2011**, *84*, 045115. [CrossRef]
189. Lieber, C.M.; Kim, Y. Characterization of the structural, electronic and tribological properties of metal dichalcogenides by scanning probe microscopies. *Thin Solid Films* **1991**, *206*, 355–359. [CrossRef]

190. Lauritsen, J.V.; Kibsgaard, J.; Olesen, G.H.; Moses, P.G.; Hinnemann, B.; Helveg, S.; Norskov, J.K.; Clausen, B.S.; Topsoe, H.; Laegsgaard, E.; et al. Location and coordination of promoter atoms in Co- and Ni-promoted MoS_2-based hydrotreating catalysts. *J. Catal.* **2007**, *249*, 220–233. [CrossRef]
191. Lewis, D.J.; Tedstone, A.A.; Zhong, X.L.; Lewis, E.A.; Rooney, A.; Savjani, N.; Brent, J.R.; Haigh, S.J.; Burke, M.G.; Muryn, C.A.; et al. Thin Films of Molybdenum Disulfide Doped with Chromium by Aerosol-Assisted Chemical Vapor Deposition (AACVD). *Chem. Mater.* **2015**, *27*, 1367–1374. [CrossRef]
192. Xie, J.F.; Zhang, J.J.; Li, S.; Grote, F.; Zhang, X.D.; Zhang, H.; Wang, R.X.; Lei, Y.; Pan, B.C.; Xie, Y. Controllable Disorder Engineering in Oxygen-Incorporated MoS_2 Ultrathin Nanosheets for Efficient Hydrogen Evolution. *J. Am. Chem. Soc.* **2013**, *135*, 17881–17888. [CrossRef] [PubMed]
193. Neal, A.T.; Pachter, R.; Mou, S. P-type conduction in two-dimensional MoS_2 via oxygen incorporation. *Appl. Phys. Lett.* **2017**, *110*, 193103. [CrossRef]
194. Yang, L.M.; Majumdar, K.; Liu, H.; Du, Y.C.; Wu, H.; Hatzistergos, M.; Hung, P.Y.; Tieckelmann, R.; Tsai, W.; Hobbs, C.; et al. Chloride Molecular Doping Technique on 2D Materials: WS_2 and MoS_2. *Nano Lett.* **2014**, *14*, 6275–6280. [CrossRef] [PubMed]
195. Liu, Q.H.; Xia, W.J.; Wu, Z.J.; Huo, J.; Liu, D.D.; Wang, Q.; Wang, S.Y. The origin of the enhanced performance of nitrogen-doped MoS_2 in lithium ion batteries. *Nanotechnology* **2016**, *27*, 175402. [CrossRef] [PubMed]
196. Kim, E.; Ko, C.; Kim, K.; Chen, Y.B.; Suh, J.; Ryu, S.G.; Wu, K.D.; Meng, X.Q.; Suslu, A.; Tongay, S.; et al. Site Selective Doping of Ultrathin Metal Dichalcogenides by Laser-Assisted Reaction. *Adv. Mater.* **2016**, *28*, 341–346. [CrossRef] [PubMed]
197. Zabinski, J.S.; Donley, M.S.; Walck, S.D.; Schneider, T.R.; McDevitt, N.T. The Effects of Dopants on the Chemistry and Tribology of Sputter-Deposited MoS_2 Films. *Tribol. Trans.* **1995**, *38*, 894–904. [CrossRef]
198. Simmonds, M.C.; Savan, A.; Pfluger, E.; Swygenhovena, H.V. Mechanical and tribological performance of MoS_2 co-sputtered composites. *Surf. Coat. Technol.* **2000**, *126*, 15–24. [CrossRef]
199. Nainaparampil, J.J.; Phani, A.R.; Krzanowski, J.E.; Zabinski, J.S. Pulsed laser-ablated MoS_2-Al films: Friction and wear in humid conditions. *Surf. Coat. Technol.* **2004**, *187*, 326–335. [CrossRef]
200. Ye, M.; Zhang, G.; Ba, Y.; Wang, T.; Wang, X.; Liu, Z. Microstructure and tribological properties of MoS_2 +Zr composite coatings in high humidity environment. *Appl. Surf. Sci.* **2016**, *367*, 140–146. [CrossRef]
201. Stoyanov, P.; Chromik, R.R.; Goldbaum, D.; Lince, J.R.; Zhang, X. Microtribological Performance of Au–MoS_2 and Ti–MoS_2 Coatings with Varying Contact Pressure. *Tribol. Lett.* **2010**, *40*, 199–211. [CrossRef]
202. Paul, A.; Singh, H.; Mutyala, K.C.; Doll, G.L. An Improved Solid Lubricant for Bearings Operating in Space and Terrestrial Environments. In Proceedings of the 44th Aerospace Mechanisms Symposium, NASA Glenn Research Center, Cleveland, OH, USA, 16–18 May 2018. NASA/CP—2018-219887.
203. Li, H.; Li, X.; Zhang, G.; Wang, L.; Wu, G. Exploring the Tribophysics and Tribochemistry of MoS_2 by Sliding MoS_2/Ti Composite Coating Under Different Humidity. *Tribol. Lett.* **2017**, *65*, 38. [CrossRef]
204. Spalvins, T. Frictional and Morphological Properties of Au-MoS_2 Films Sputtered from a Compact Target. *Metall. Prot. Coat.* **1984**, *118*, 375–384. [CrossRef]
205. Scharf, T.W.; Kotula, P.G.; Prasad, S.V. Friction and wear mechanisms in MoS_2/Sb_2O_3/Au nanocomposite coatings. *Acta Mater.* **2010**, *58*, 4100–4109. [CrossRef]
206. Scharf, T.W.; Goeke, R.S.; Kotula, P.G.; Prasad, S.V. Synthesis of Au-MoS_2 nanocomposites: Thermal and friction-induced changes to the structure. *ACS Appl. Mater. Interfaces* **2013**, *5*, 11762–11767. [CrossRef] [PubMed]
207. Lince, J.R.; Kim, H.I.; Adams, P.M.; Dickrell, D.J.; Dugger, M.T. Nanostructural, electrical, and tribological properties of composite Au–MoS_2 coatings. *Thin Solid Films* **2009**, *517*, 5516–5522. [CrossRef]
208. Ding, X.Z.; Zeng, X.T.; He, X.Y.; Chen, Z. Tribological properties of Cr- and Ti-doped MoS_2 composite coatings under different humidity atmosphere. *Surf. Coat. Technol.* **2010**, *205*, 224–231. [CrossRef]
209. Singh, H.; Mutyala, K.C.; Mohseni, H.; Scharf, T.W.; Evans, R.D.; Doll, G.L. Tribological Performance and Coating Characteristics of Sputter-Deposited Ti-Doped MoS_2in Rolling and Sliding Contact. *Tribol. Trans.* **2015**, *58*, 767–777. [CrossRef]
210. Hsu, W.K.; Zhu, Y.Q.; Yao, N.; Firth, S.; Clark, R.J.H.; Kroto, H.W.; Walton, D.R.M. Titanium-doped molybdenum disulfide nanostructures. *Adv. Funct. Mater.* **2001**, *11*, 69–74. [CrossRef]
211. Singh, H.; Mutyala, K.C.; Evans, R.D.; Doll, G.L. An atom probe tomography investigation of Ti–MoS_2 and MoS_2–Sb_2O_3–Au films. *J. Mater. Res.* **2017**, *32*, 1710–1717. [CrossRef]

212. Li, H.; Zhang, G.; Wang, L. The role of tribo-pairs in modifying the tribological behavior of the MoS_2/Ti composite coating. *J. Phys. D Appl. Phys.* **2016**, *49*, 095501. [CrossRef]
213. Lince, J.R. Tribology of co-sputtered nanocomposite Au/MoS_2 solid lubricant films over a wide contact stress range. *Tribol. Lett.* **2004**, *17*, 419–428. [CrossRef]
214. Singh, H.; Mutyala, K.C.; Evans, R.D.; Doll, G.L. An investigation of material and tribological properties of Sb_2O_3/Au-doped MoS_2 solid lubricant films under sliding and rolling contact in different environments. *Surf. Coat. Technol.* **2015**, *284*, 281–289. [CrossRef]